Lithos 266–267 (2016) 309–331

Contents lists available at ScienceDirect

Lithos

journal homepage: www.elsevier.com/locate/lithos

High-pressure greenschist to blueschist facies transition in the Maimón Formation (Dominican Republic) suggests mid-Cretaceous subduction of the Early Cretaceous Caribbean arc

L. Torró [a,*], A. Garcia-Casco [b,c], J.A. Proenza [a], I.F. Blanco-Quintero [d], G. Gutiérrez-Alonso [e], J.F. Lewis [f]

[a] Departament de Mineralogia, Petrologia i Geologia Aplicada, Facultat de Geologia, Universitat de Barcelona (UB), Martí i Franquès s/n, 08028 Barcelona, Spain
[b] Departamento de Mineralogía y Petrología, Universidad de Granada, Fuentenueva s/n, 18002 Granada, Spain
[c] Instituto Andaluz de Ciencias de la Tierra, CSIC-UGR, Av. las Palmeras, 4, 18100 Armilla, Granada, Spain
[d] Departamento de Geociencias, Universidad de los Andes, Bogotá, Colombia
[e] Departamento de Geología, Universidad de Salamanca, 37008 Salamanca, Spain
[f] Department of Earth and Environmental Sciences, George Washington University, Washington, DC 20052, USA

ARTICLE INFO

Article history:
Received 26 July 2016
Accepted 24 October 2016
Available online 29 October 2016

Keywords:
Blueschist
HP/LT metamorphism
Maimón Formation
Dominican Republic
Caribbean
Volcanic arc

ABSTRACT

The Maimón Formation (Cordillera Central, Dominican Republic) is formed of metamorphosed bi-modal mafic-felsic volcanic rocks and sedimentary horizons of Early Cretaceous age deposited in the forearc of the nascent Caribbean island arc. Two structural-metamorphic zones depict an inverted metamorphic gradient: the Ozama shear zone, which records intense mylonitic and phyllonitic deformation and ubiquitous metamorphic recrystallization, tectonically overlies the much less deformed and variably recrystallized rocks of the El Altar zone. The presence of ferri-winchite and high-Si phengite, first reported in this paper, in the peak metamorphic assemblage of rocks of the Ozama shear zone (actinolite + phengite + chlorite + epidote + quartz + albite ± ferri-winchite ± stilpnomelane) point to subduction-related metamorphism. Pseudosection calculations and intersection of isopleths indicate peak metamorphic conditions of ~8.2 kbar at 380 °C. These figures are consistent with metamorphism in the greenschist/blueschist facies transition, burial depths of ~25–29 km and a thermal gradient of ~13–16 °C/km. Our new data dispute previous models pointing to metamorphism of Maimón rocks under a steep thermal gradient related to burial under a hot peridotite slice. Instead, we contextualize the metamorphism of the Maimón Formation in a subduction scenario in which a coherent slice of the (warm) Early Cretaceous forearc was engulfed due to intra-arc complexities and regional-scale-driven tectonic processes operating in the late Early Cretaceous. Integration of our findings with previous studies on metamorphic complexes in Hispaniola suggests that a major tectonic event affecting the whole arc system took place at c. 120–110 Ma.

1. Introduction

Intra-oceanic island arc systems represent locus of intense magmatism and seismic activity coupled to major metamorphic and tectonic processes framed in a rapidly evolving setting relative to other geological systems (Gerya, 2011; Gerya et al., 2002; Ichikawa et al., 2016; Maresch and Gerya, 2005). Despite having a simple crustal structure when compared to arcs developed on continental crust (e.g., Jicha and Jagoutz, 2015; Stern, 2010), intra-oceanic arcs ordinarily embrace complex, condensed in time and space, tectonic processes that may couple extension and compression along a single arc involving the trench, forearc, volcanic-magmatic arc and back-arc (Hawkins et al., 1984). Formed in dynamic subduction systems, these arcs are the loci for the development of high-pressure, low-temperature (HP/LT) metamorphism, whose study offers a priceless information on the evolution of convergent plate margins (e.g., Agard et al., 2009). In the Greater Antilles, in the northern margin of the Caribbean plate, several of these HP-LT metamorphic complexes have been studied in Cuba (e.g., Blanco-Quintero et al., 2010; Boiteau et al., 1972; Garcia-Casco et al., 2002, 2006, 2008a, 2008b; Millán, 1996; Schneider et al., 2004; Stanek et al., 2006) and Jamaica (e.g., West et al., 2014; Willner et al., 2016). In Hispaniola (Haiti and Dominican Republic), HP/LT metamorphic complexes include Samaná (Escuder-Viruete et al., 2011) and Río San Juan (Escuder-Viruete and Pérez-Estaún, 2013; Escuder-Viruete et al., 2013a, 2013b; Krebs et al., 2008, 2011). Subduction/exhumation and associated prograde/retrograde metamorphism recorded on these Antillean complexes are dated as Cretaceous. In Cuba, serpentinite-matrix mélanges record subduction of MOR-

* Corresponding author at: Departament de Mineralogia, Petrologia i Geologia Aplicada, Universitat de Barcelona, C/ Martí i Franquès s/n, 08028 Barcelona, Catalunya, Spain.
E-mail address: lisardtorro@hotmail.com (L. Torró).

http://dx.doi.org/10.1016/j.lithos.2016.10.026
0024-4937/

derived material since the Early Cretaceous (e.g., Blanco-Quintero et al., 2011; Garcia-Casco et al., 2002, 2006; Lázaro et al., 2009). In the Río San Juan metamorphic complex, oceanic crust including MOR- and island-arc-derived materials begun to subduct in the Early Cretaceous (Escuder-Viruete et al., 2013b); therefore, initial intra-arc complexities during the first stages of subduction in the Hispaniola segment of the Caribbean island arc must be pondered on any model regarding initial subduction geometry below the primitive, Hauterivian-Albian Caribbean island arc (cf. Lidiak and Anderson, 2015; Pindell et al., 2012).

Uplift and unroofing after Neogene tectonics bountifully expose deformed and metamorphosed Early Cretaceous basement rocks along the Median Belt in Cordillera Central (sensu Lewis and Draper, 1990) of Hispaniola. Therefore, the Median Belt renders an exceptional opportunity to study deformation and metamorphic processes that affected geologic units during the first stages of the tectonic evolution of the Caribbean Island Arc. The study of the metamorphic units (including the Maimón and Amina Formations and the Río Verde and Duarte complexes) and the conspicuously complex structure has led to the construction of regional-scale tectonic models on the early evolution of the Caribbean island arc. Such models include, for example, the proposal of a paired metamorphic belt in Hispaniola unlike the rest of the Greater Antilles (Nagle, 1974) and an Aptian/Albian subduction polarity reversal event under the primitive arc (e.g., Draper and Gutiérrez-Alonso, 1997; Draper and Lewis, 1991; Draper et al., 1996; Lebrón and Perfit, 1994; Lewis et al., 2002).

The metamorphic grade undergone by the Maimón Formation has been recurrently classified as of low-pressure greenschist facies on the basis of the petrographic study of its metamorphic mineral assemblages (Bowin, 1960, 1966; Draper and Gutiérrez-Alonso, 1997; Draper and Lewis, 1991; Draper et al., 1996; Escuder-Viruete et al., 2002; Kesler et al., 1991a; Nagle, 1974); nevertheless, these studies largely lacked methodical mineral chemical analysis. In the course of a petrological and geochemical characterization of rocks from this formation, we found unexpected systematic high Si contents in white mica lepidoblasts and presence of the sodium-calcium amphibole ferriwinchite in rocks from the Ozama shear zone, suggestive of moderate pressures of crystallization. This article presents, for the first time, an exhaustive study on the petrology and mineral chemistry of metamorphic assemblages of rocks from the Maimón Formation. We offer isochemical P–T projections (pseudosection) in order to constrain the P–T evolution undergone by the studied rocks and to discuss their meaning by comparison to previous work in the context of subduction-zone thermal gradients. In addition, we assert the influence of the intense pre-metamorphic hydrothermal alteration of the rocks in the subsequent metamorphic assemblages and show that diagnostic high-P assemblages are expected to form only in the less intensely altered rocks. The existence of high-pressure subduction-related mineral assemblages in rocks of the Maimón Formation is not only of local interest, but has major implications for the interpretation of early geodynamic evolution of the Caribbean realm.

2. Geological overview

The island of Hispaniola is a collage of Early Cretaceous to Tertiary arc-, oceanic- and continental margin-derived units which resulted largely from the oblique convergence and underthrusting of the North American (Proto-Caribbean) Plate beneath the Greater Antilles island-arc since c. 135 Ma (Pindell et al., 2012; Rojas-Agramonte et al., 2011). Mesozoic separation of North and South America allowed the progressive west to east insertion into the Proto-Caribbean (Atlantic) realm of the allochthonous (Pacific in origin) Caribbean plate and related arc and oceanic complexes (Boschman et al., 2014; Lidiak and Anderson, 2015 and references therein; Pindell and Kennan, 2009). West-dipping subduction of the Proto-Caribbean caused arc–continent collision in the northern leading edge of the Caribbean in the latest Cretaceous-earliest Tertiary and obduction of ophiolitic complexes onto continental margins in Guatemala, Cuba, Hispaniola and Puerto Rico (Garcia-Casco et al., 2008a; Lewis et al., 2006; Pindell et al., 2012; Solari et al., 2013). In Hispaniola, subduction and related arc-magmatism ceased after the collision with the Bahamas platform in Eocene time (Donnelly et al., 1990; Mann et al., 1991), and the plate margin evolved to the current left-lateral strike-slip tectonics (Mann et al., 2002; Vila et al., 1987).

The Early Cretaceous Maimón Formation is a 9 km wide and about 73 km long NW-SE trending belt that crops out along the Median Belt (Central Cordillera) of the Dominican Republic (Draper and Lewis, 1991; Kesler et al., 1991a). The Median belt is a composite of accreted oceanic units affected by the left-lateral strike-slip Hispaniola (HFZ) and San Juan-Restauración (SJRFZ) fault zones (Fig. 1a)

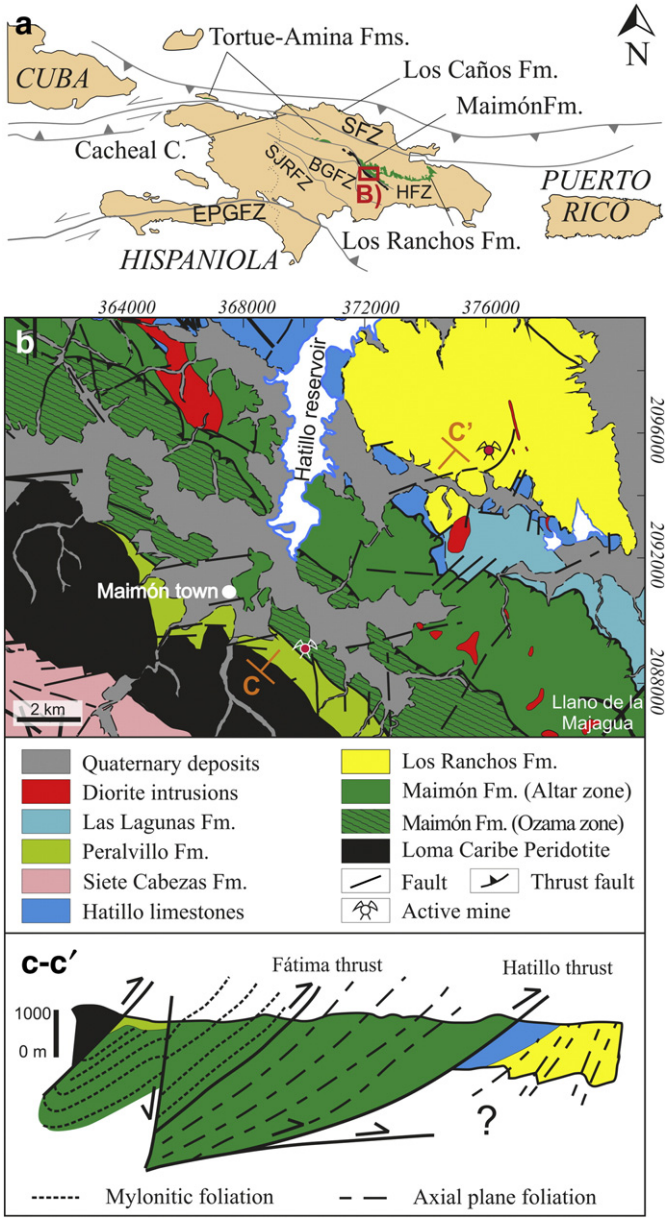

Fig. 1. (a) Location of the PIA series (green), ophiolitic peridotites (black), and major fault zones of Hispaniola; EPGFZ: Enriquillo-Plantain Garden fault zone; SFZ: Septentrional fault zone; HFZ: Hispaniola fault zone; BGFZ: Bonao-La Guácara fault zone; SJRFZ: San Juan-Restauración Fault Zone. (b) Geological map of the Maimón Formation and surrounding units modified from Martín and Draper (1999). (c-c′) Synthetic geologic cross section of the Maimón Formation and surrounding geologic units in the Median belt. (After Draper et al., 1996.)

(Escuder-Viruete et al., 2008). The Maimón Formation is in steep fault contact with the Loma Caribe peridotite (Fig. 1b–c) (Escuder-Viruete et al., 2007a; Lewis et al., 2002). However, the Loma Caribe peridotite belt is locally separated from the Maimón Formation at their southern contact by the Peralvillo Sur Formation, a thin sequence of undeformed and unmetamorphosed arc-related volcanic and volcanosedimentary rocks of Late Cretaceous (?) age (Lewis et al., 2000; Martín and Draper, 1999). To the northeast, the Maimón Formation limits with the Los Ranchos Formation, a volcanic pile of bimodal volcanic, volcaniclastic and minor sedimentary rock units. The Early Cretaceous volcanic-arc Maimón and Los Ranchos formations are overlain by the late lower Albian shallow-water reefal Hatillo limestone (Kesler et al., 2005). Recent, post-Early Eocene (Draper et al., 1996) tectonics juxtaposed the Maimón Formation over the Hatillo limestone along the Hatillo Thrust (Fig. 1c). Both the Maimón and Hatillo Formations are intruded by diorite dykes and plugs of Paleocene (?) age (Bowin, 1966; Martín and Draper, 1999). Rocks from the Maimón Formation are characterized by the development of syn-metamorphic ductile fabrics and structures. As described by Draper et al. (1996) and Draper and Gutiérrez-Alonso (1997), the intensity of ductile deformation and metamorphic grade increases towards the SW of the Maimón belt, as observed particularly well in the Ozama shear zone (Fig. 1b), which occupies the uppermost level of the structural sequence (Fig. 1c). Deformation and metamorphism is much less intense to the NE half of the Maimón belt (i.e., the so-called El Altar zone, to the NE of the Fátima thrust fault Fig. 1b–c). Although rocks in the El Altar zone vary from fully recrystallized to weakly metamorphosed and even slightly undeformed across this trend, a pronounced change in the intensity of metamorphic recrystallization and deformation is observed on each side of the Fátima thrust fault.

The Maimón Formation is composed of bimodal mafic-felsic volcanic and volcaniclastic rocks and a thin belt of well-laminated rocks of sedimentary origin that is conformable with the volcanic sequence; the sedimentary rocks crop out in the north central part of the formation and include well laminated fine-grained meta-tuffs, dark graphite-shales, cherts and limestones (Kesler et al., 1991a; Lewis et al., 2000). The volcanic rocks of the Maimón Formation are representative of the oldest and chemically most primitive island-arc volcanism in the Caribbean region (Escuder-Viruete et al., 2007b, 2010; Lewis and Draper, 1990; Lewis et al., 2002), commonly referred to as Primitive Island Arc (PIA/IAT) series (e.g., Jolly et al., 2001 and references therein). Recently, Torró et al. (2016, in press) classified the basalts from the Maimón Formation as LREE-depleted low-Ti island arc tholeiites, boninites and less abundant low-Ti island-arc tholeiites (LOTI) and identified mantle-type (M-type), boninitic and tholeiitic signatures in the low-K felsic volcanic rocks. Similar lithotypes were described by Escuder-Viruete et al. (2007b) for the Amina Formation, which is considered a separate segment of the same igneous protoliths and metamorphic belt. On the basis of the lithogeochemistry and magmatic relations, these workers suggest that the formation of Maimón took place in a forearc environment just after the subduction initiation of the Proto-Caribbean oceanic basin in the Early Cretaceous (>126 Ma) related to initial extensive regime in the fore-arc.

3. Material and methods

This study develops from a total of 182 drill core and surface field rock samples representative of the volcanosedimentary materials of the Maimón Formation in its south-central section (approx. from the Hatillo dam to the Ozama River near el Llano and la Majagua; Fig. 1b). A petrographic study was carried out on 45 thin sections by means of optical microscopy with transmitted and reflected light and by electronic microscopy using an environmental SEM Quanta 200 FEI, XTE 325/D8395 equipped with an INCA Energy 250 EDS microanalysis system equipment at the Serveis Científics i Tecnològics of the University of Barcelona and a Quanta 400 FEI equipped with a Bruker xFLash 6/30EDS microanalysis system at the Centro de Instrumentación Científica of the University of Granada. Based on this study, 11 samples were selected for mineral chemical measurements.

Mineral analyses were performed using a JEOL JXA-8230 electron microprobe (EMP) at the Serveis Científics i Tecnològics of the University of Barcelona, operated at 20 kV acceleration voltage, 15 nA beam current and with a beam diameter of 5 μm. Analytical standards and lines used for analyses were wollastonite (Si Kα; Ca Kα), corundum (Al Kα), AgCl (Cl Kα), fluorite (F Kα), albite (Na Kα), periclase (Mg Kα), Fe_2O_3 (Fe Kα), rhodonite (Mn Kα), orthoclase (K Kα), rutile (Ti Kα). The PAP correction procedure was used (Pouchou and Pichoir, 1985). The same instrument operated at 20 kV and 300 nA, with a focused beam, a step (pixel) size of 4 μm, and a counting time of 30 ms/pixel was used to obtain elemental (Si, Al, Ti, Fe, Mg, Mn, Ca, Na, K, Ba) X-ray maps. The X-ray maps were processed with software DWImager (Torres-Roldán and Garcia Casco, unpublished) and consist of the X-ray signals of the elements or element ratios (color-coded; expressed in counts/nA per s); voids, polish defects and mineral phases other than amphibole were masked out and overlain onto a gray-scale SEM-BSE image which contains the basic textural information of the scanned areas (see Garcia-Casco, 2007). Spot analyses were performed on points selected using the X-ray maps and in other significant samples (Tables 2–5).

Mica and chlorite were normalized to 11 and 14 O, respectively, and $Fe_{total} = Fe^{2+}$. Amphibole compositions were normalized to 23 O, H_2O was determined by assuming (OH + F + Cl) = 2 a.p.f.u., and the distribution of cations in the A-, B-, C- and T-sites was carried out by stoichiometry following the scheme of Hawthorne et al. (2012); for amphiboles, Fe^{3+} was estimated for electroneutrality after cation normalization according to stoichiometric constraints proposed by Hawthorne et al. (2012). Epidote was normalized to 3 Si, and plagioclase to 8 O, both with $Fe_{total} = Fe^{3+}$. Mineral and end-member abbreviations are after Whitney and Evans (2010), completed with those proposed by Hawthorne et al. (2012) for amphiboles, and abbreviations of end-members of phases are written entirely in lower case. The atomic concentration of elements per formula units is abbreviated a.p.f.u. The atomic ratio $Mg/(Mg + Fe^{2+})$ is termed Mg#.

The triangular ACF, AKF and AFM, and the tetrahedral AFMN- and ACFN-deluxe diagrams were constructed after projection of chemical compositions from phases and exchange vectors following algebraic methods (Singular Value Decomposition, Fisher, 1989, 1993) using software CSpace (Torres-Roldán et al., 2000). The diagrams contain the composition of analyzed minerals and bulk rocks and of representative end-members of solid solutions projected from phases and exchange vectors as indicated in Figs. 4, 5 and 12. In these diagrams, Fe is treated as $Fe^{2+}{}_{total}$ since the amounts of Fe^{2+} and Fe^{3+} in micas and chlorite cannot be estimated by stoichiometry. The manipulation of the composition space by means of exchange vectors results in condensation that allows for consideration of all analyzed elements at once in the diagram. However, since the number of chemical components of the system is artificially reduced after algebraic constraining, the condensation process produces artificial degeneracy, making particular end-members of variable composition to plot in the same position in the diagram (i.e., for plotting purposes, they are indistinguishable). For the same reason, some chemical variations in the analyzed minerals cannot be resolved (e.g., K vs Na, Fe vs Mg in the ACFN diagram). In spite of these inconveniences, the AFMN- and AKFM-deluxe diagrams are nevertheless convenient for simultaneous inspection of mineral assemblages in a single rock sample and for important chemical variations of the coexisting minerals and rocks.

The thermodynamic calculations (pseudosection) in the KNCFMASHO (K_2O-Na_2O-CaO-FeO-MgO-Al_2O_3-SiO_2-H_2O-O_2) system were performed using the Perple_X software (Connolly, 1990, 2005). A fluid phase, assumed to be pure H_2O, was considered in excess. The oxygen contents for transformations of ferrous to ferric iron was chosen (at 10 M percent) after some preliminary calculations in order to reproduce the presence of epidote in key assemblages stable within the P–T window of interest and

the calculated content of trivalent iron in most minerals. Our procedure (test-value calculations) follows that of Willner et al. (2016) and other workers. The solution models used for amphibole, feldspar, clinopyroxene, chlorite, white mica and epidote are those of Dale et al. (2005), Fuhrman and Lindsley (1988), Green et al. (2007), Holland et al. (1998), Coggon and Holland (2002), and Holland and Powell (1998), respectively. Alternative solid solution models for amphibole (e.g., Massonne and Willner, 2008) were tested; however, they failed to reproduce the observed mineral assemblage of the studied samples (e.g., they indicate stabilization of clinopyroxene, which is not present in studied rocks, at all conditions in the P–T window of interest).

4. Microstructures

Rocks from the Maimón Formation are characterized by development of syn-metamorphic ductile fabrics and structures. However, and as described by Draper et al. (1996) and Draper and Gutiérrez-Alonso (1997), a trend towards increasing internal deformation and metamorphic grade is observed to the SW of the Maimón belt, particularly in the Ozama shear zone (Fig. 1b; i.e., in the uppermost levels of the structural sequence, Fig. 1c); deformation is much less intense to the NE half of the Maimón belt (i.e., the so-called El Altar zone, to the NE of the Fátima thrust fault). Although rocks vary from fully recrystallized to weakly metamorphosed and undeformed along this trend, a pronounced change in the metamorphic recrystallization and deformation degrees is observed on each side of the Fátima thrust fault and hence both zones are described separately.

4.1. Ozama shear zone

Rocks of the Ozama shear zone include greenschists and scarce gneissic low-K meta-plagiorhyolites. The samples are pervasively deformed and recrystallized and lack magmatic remnants (Fig. 2). Though the abundance of minerals diverge as a function of bulk-rock composition (Fig. 5), in both types of rock the metamorphic parageneses are formed mostly by chlorite, muscovite (s.l.; phengite *s.s.*, see below), epidote, amphibole (actinolite ± ferri-winchite, see below), albite, stilpnomelane and quartz. Opaque accessory minerals include disseminations of sulfides (mainly sub-euhedral pyrite) and trace minute (~10 μm in size) titanite and rutile grains. Recrystallization and deformation developed mylonitic structures and planar fabrics defined by muscovite, muscovite-chlorite intergrowths, amphibole and a crenulation metamorphic compositional layering (Fig. 2). Meso- and micro-scale petrographic observations reveal three deformation events (D_{p-1}, D_p and D_{p+1}, where D_p refers to the principal deformation event). D_{p-1} resulted in the development of a S_{p-1} foliation locally preserved in muscovite and muscovite ± chlorite microlithons located in mm- to cm-scale domains between lepidoblastic muscovite sheets defining the main crenulation cleavage (S_p; Fig. 2e–f); they are also preserved in dm-scale fold hinges, mostly isoclinal, with extremely attenuated or inexistent limbs developed mostly in the most felsic (quartz bearing) lithologies and fold axis depicting a great circle parallel to the S_p foliation. D_p tectonic layering development corresponds with peak metamorphism (recrystallization) and involved the almost complete obliteration of the magmatic and previous deformation features. The associated schistosity (S_p) is planar (Fig. 2a) and locally, slightly anastomosed, often resulting in compositional layering (Fig. 2b,c,g). The orientation of this foliation is quite uniform, SW trending and dipping ~60° to the south. Foliation surfaces show occasionally a mineral stretching lineation plunging 25°–35° towards the S–SSW. Metamorphic compositional layering is defined by alternating centimeter- to submillimeter-wide albite–quartz, muscovite-chlorite- and actinolite-rich layers preserving previous S_{p-1} in the crenulation hinges (Fig. 2g). Poorly developed submillimeter-scale S-C and mica-fish fabrics are also observed in samples with higher phyllonitic character. Deformation stages and foliations S_{p-1} and S_p may correspond to progressive deformation under the same deformation regime. Finally, a deformation stage D_{p+1} generated folding of the previous structures and development of an incipient S_{p+1} foliation (Fig. 2b–d). D_{p+1} folds are mainly isoclinal and doubly verging (Fig. 2b), if more complex patterns embrace parasitic (second order) symmetric and asymmetric, disharmonic (Fig. 2b–c) or sheath folds (Fig. 2d) typical of ductile (mylonitic) shear zones (e.g., Carreras et al., 2005). Thin, millimeter- to centimeter-wide quartz veins are common in the Ozama shear zone, occurring mostly parallel and jointly folded with S_p foliation, and are affected by shearing, asymmetrical disharmonic folding and extension evidenced by boudinage parallel to the S_p (Fig. 2b,g).

Preferred orientation of quartz ribbons and of the variably elongated quartz, albite and epidote porphyroclasts is characteristic of the Ozama shear zone rocks, and define, along with the muscovite, chlorite and amphibole lepidoblasts, a planar-linear (S_p-L_p) fabric. Polycrystalline quartz porphyroclasts systematically develop asymmetric σ-type shear structures composed of very fine-grained quartz and chlorite/muscovite wrapped by muscovite-chlorite-amphibole lepidoblasts of the S_p foliation (Fig. 2h). Quartz shows marked undulose extinction and internal stylolitic joints. Epidote concentrates in rocks of mafic protoliths (Torró et al., 2016, in press), with local concentrations higher than 50% modal constituting meta-epidosites. Even if most of epidote crystallization probably resulted from the spilitization of the basalts (cf. Gilgen et al., 2016), deformed epidote crystals displaying fan-like textures (Fig. 2i) and adjacent helical poikiloblastic zones (recalling snowball textures) and δ-type shear structures (Fig. 2j) suggest syntectonic rotational blastesis. Eventually, ultramylonites developed after the gneissic meta-rhyodacites close to the Fátima thrust, where monocrystalline, variably comminuted quartz porphyroclasts of millimetric to submillimetric diameter occur in a very fine-grained quartz-muscovite matrix.

Sulfides in the volcanogenic massive sulfide lenses hosted in the Ozama shear zone also record intense mylonitic deformation. In the outer limits of the sulfide lenses, rotated pyrite porphyroclasts develop asymmetrical pressure shadows composed of feather-shaped quartz crystals and envelopes of extremely elongated chalcopyrite-sphalerite crystals. For a detailed description of the deformation/recovery textures recorded in the Cerro de Maimón VMS sulfides, the reader is referred to Torró et al. (2016).

According to the observed kinematic criteria in the observed porphyroclasts and the study of the quartz <c> axis orientations (CPOs, Draper and Gutiérrez-Alonso, 1997) in the S_p quartz ribbons described above, the shear sense obtained indicates a top to the N-NE sense of movement in agreement with a thrusting-transpressional deformation regime.

4.2. El Altar zone

Northeast of the Fátima thrust, at its footwall, rocks from the El Altar zone are characterized by remarkably less intense ductile deformation and penetrative foliation than rocks from the Ozama shear zone, and by limited metamorphic recrystallization (Fig. 3); a continuous spectrum of deformation and metamorphic recrystallization is distinguished from the incipient protomylonites identified near the Fátima thrust to the undeformed and metamorphically unaffected rocks from the far NW section of the Maimón Formation (Fig. 3a). The prevalence of meta-plagiorhyolites over meta-basalts and the occurrence of a metasedimentary sequence some tens of meters thick are also distinctive features of this zone. Phengite and chlorite are the main metamorphic phases along with less abundant epidote and paragonite. Minor and trace proportions of magnetite, hematite, apatite, rutile and titanite (not present in all samples) are observed.

Incipient protomylonitic fabrics developed in meta-basalts and meta-plagiorhyolites show penetrative anastomosed to planar foliation defined by muscovite and minor chlorite lepidoblasts that crudely adapts around igneous/hydrothermal(?) plagioclase (Fig. 3f–g) and

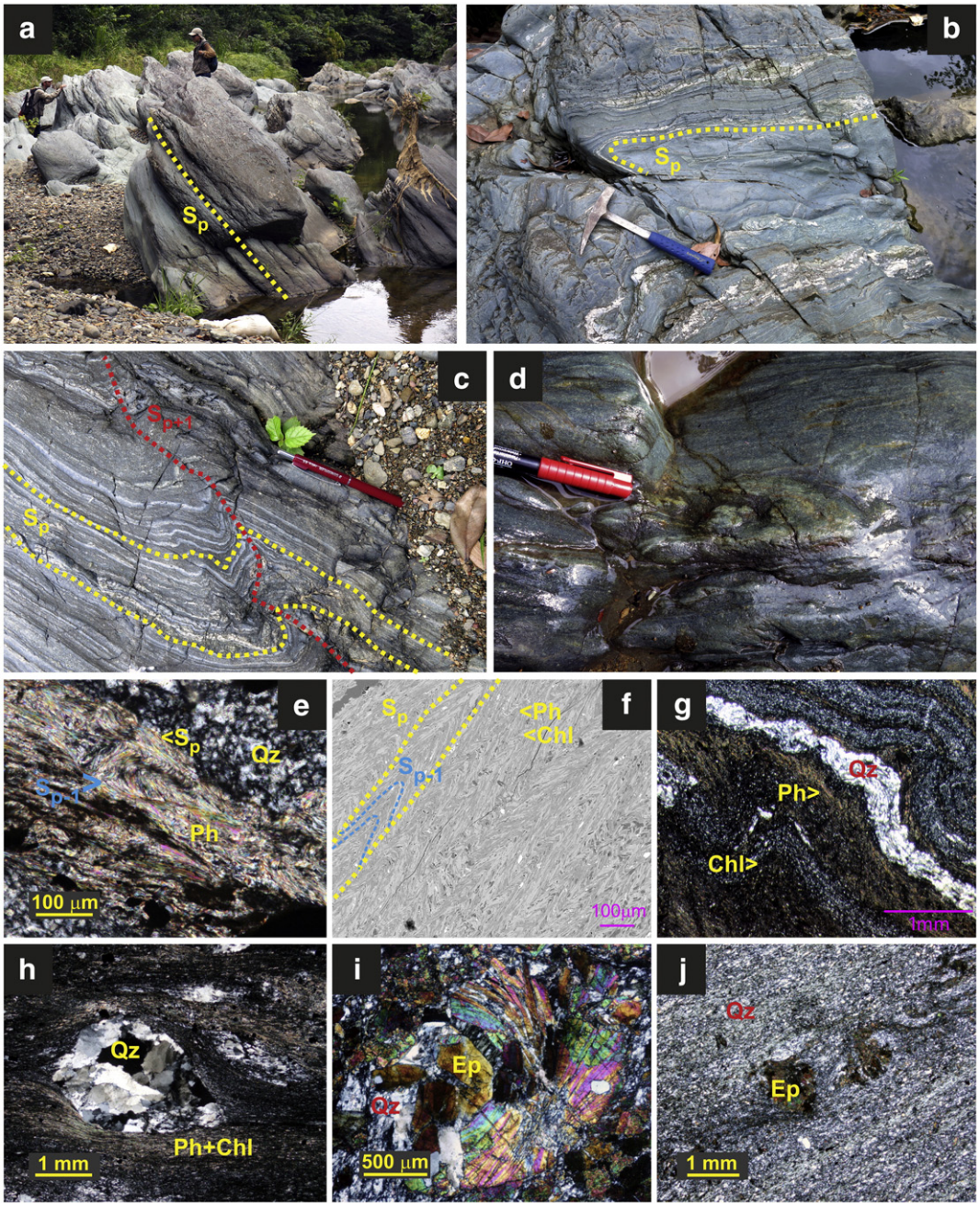

Fig. 2. Field aspect (a–d) and microphotographs (e–j) of rocks from the Ozama shear zone, Maimón Formation. (a) Outcrop of greenschists in the Ozama River with marked planar foliation (S_p). (b) Detail of schist outcrop showing D_p isoclinal folding of the compositional layering and the quartz veins which are sheared, asymmetrically folded and boudinaged parallel to the S_p. (c) Metamorphic compositional layering (foliation S_p) given by the alternation of millimeter- to centimeter-wide bright and dark layers folded by a D_{s+p} deformation stage which developed an incipient S_{p+1} foliation. (d) Folded mylonitic foliation and centimeter-scale sheath (closed) folds. (e) S_{p-1} in muscovite microlithon enveloped by S_p muscovite sheets in a fine grained quartz matrix (crossed polars). (f) Detail of tightly micro-folded muscovite-chlorite intergrowths defining S_{p-1} and S_p defined by muscovite sheets concentrated along the limbs of the folds (SEM-BSE image). (g) Metamorphic compositional layering of alternating submillimeter-wide muscovite-chlorite layers and very fine-grained quartz layers along with occasional parallel boudinaged quartz veins; crenulation cleavage is locally developed (crossed polars). (h) Quartz porphyroclast showing ribbon texture with σ-type structure composed of very-fine quartz enveloped by muscovite in mylonitized schist; note the strong undulose extinction of the quartz crystals in the quartz ribbon (crossed polars). (i) Deformed epidote crystals displaying fan-like textures in meta-epidosite (crossed polars). (j) Epidote porphyroclasts in a fine-grained quartz matrix showing helical poikiloblastic zones (snowball-like) and δ-type structure evidencing syntectonic rotational blastesis and deformation (crossed polars).

quartz (Fig. 3b, h–i) porphyroclasts describing symmetric (Fig. 3f–g) to locally weakly asymmetrical (Fig. 3h) ribbons. The orientation of the rough cleavage present in this zone is parallel to the shear foliation of the Ozama zone. The development of symmetric pressure shadows composed of very fine-grained quartz adjacent to quartz porphyroclasts is limited (Fig. 3i). Mineral or stretching lineation in the protomylonites of the el Altar zone is broadly absent (Fig. 3f–g, i).

CPOs in the quartz-rich rocks of the Altar zone, close to the Fátima thrust (Draper and Gutiérrez-Alonso, 1997) depict girdles compatible with pure-shear deformation, in contrast with those in the Ozama zone, revealing different deformation mechanisms in both zones.

General preservation of the protolith magmatic textures and mineralogy allows their classification as fine plagioclase- and pyroxene-phyric, massive basalts (Fig. 3d, f–g, j–k) and highly fine to medium-grained

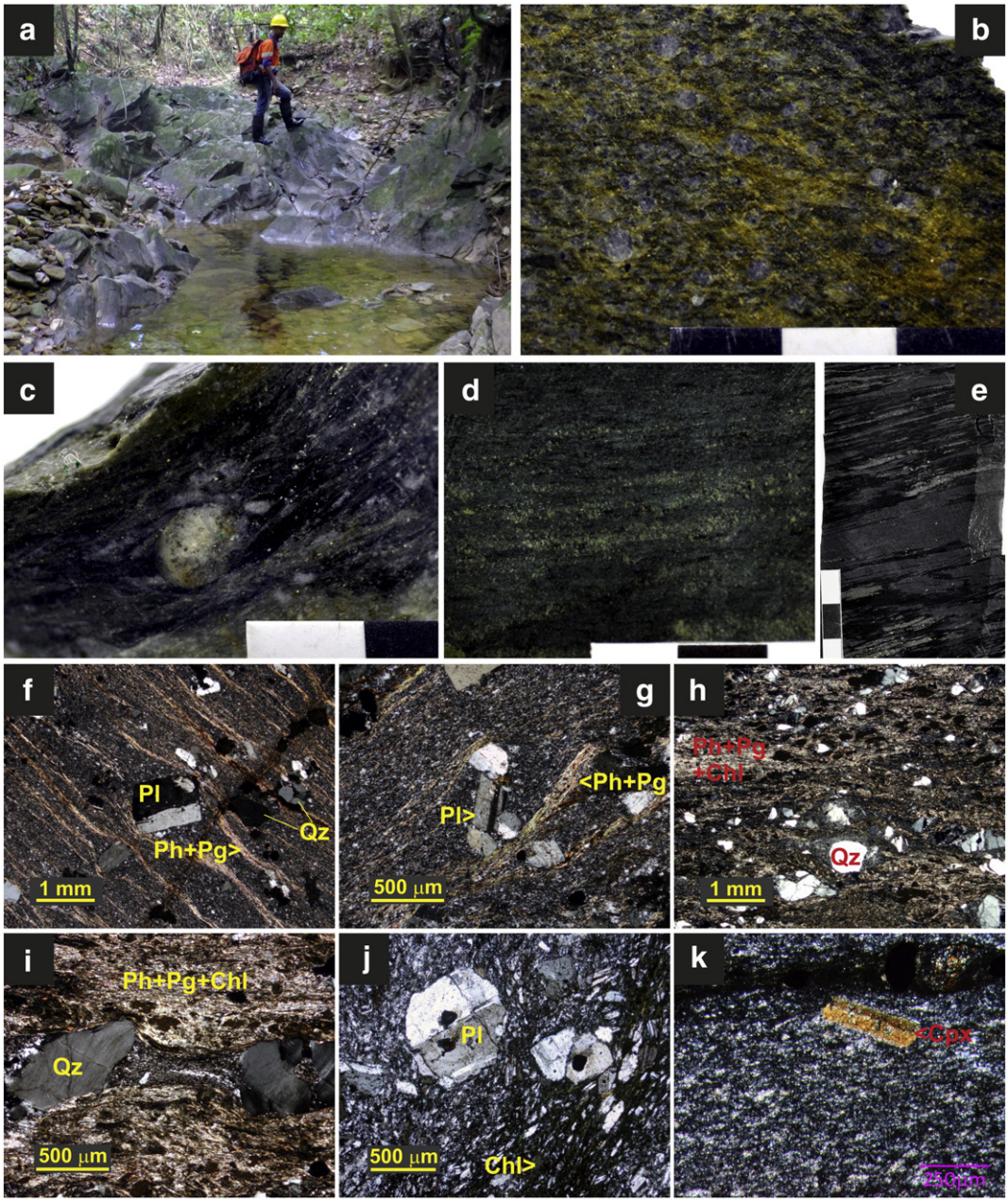

Fig. 3. Field outcrop (a), hand sample (b–e) and photomicrographs (transmitted light and crossed polars; f–k) of rocks from the El Altar zone, Maimón Formation. (a) Meta-rhyodacite outcrop in the Palo de Cuaba stream; note the general low deformation of the rocks, which is limited to coarse cleavage. (b) Millimeter-sized quartz porphyroclasts enveloped by crude and anastomosed foliation in a meta-rhyodacite sample. (c) Pyritized, poorly deformed thinly bedded rhyodacite lava sample found close to the Fátima thrust fault in the Loma la Mina area; flow layers (with alternating pale siliceous and partially recrystallized and chloritized glassy matrix layers) adapts around a rounded quartz phenocryst. (d) Chloritized and epidotitized, poorly deformed, fine plagioclase- and pyroxene-phyric, massive boninitic basalt (Torró et al., 2016). (e) Graphite-shale developed on carbonaceous sediments along the Maimón Fm. sedimentary unit, close to the Fátima thrust; note pyrite dissemination and the presence of quartz veins along the planar foliation of the rock. (f–g) Muscovite lepidoblasts describing planar to anastomosed penetrative foliation that mildly wrap around plagioclase and minor quartz phenocrysts in a semi-porphyritic meta-basalt; note the absence of pressure shadows and the preferred orientation of the phenocrysts. (h) Meta-rhyodacite with abundant and variably fragmented quartz phenocrysts in a fine grained quartz-rich matrix; a crude foliation is defined by muscovite-chlorite lepidoblasts. (i) Detail of pressure shadow of fine-grained quartz adjacent to two quartz phenocrysts in a fine-grained matrix composed of quartz and muscovite-chlorite; note the absence of preferred orientation or lineation of the quartz phenocrysts. (j) Poorly deformed, moderately fine to medium plagioclase-phyric, massive basalt; the matrix is composed of fine-grained plagioclase crystals and chloritized glass. (k) Pyroxene phenocryst remnant in protomylonite; sample collected very close to the Fátima thrust.

quartz-phyric massive plagiorhyolites (Fig. 3b–c, h–i). Plagioclase porphyroclasts are elongated and develop local asymmetric pressure shadows; breaking apart and subtle antithetical bookshelf rotation of plagioclase fragments is common. Flow layering (with alternating pale siliceous and partially recrystallized and chloritized glassy matrix layers) adapting around rounded quartz porphyroclasts is locally preserved (Fig. 3c). In undeformed metamorphically unaffected porphyritic basalts, the matrix is observed to be made up of chloritized volcanic glass along with fine-grained plagioclase laths (Fig. 3d, j). Chloritized volcanic glass is also detected in moderately amygdaloidal clasts of the less abundant meta-hyaloclastites; these rocks display jigsaw-fit and clast-in-matrix textures suggesting in situ quench fragmentation.

Sedimentary rocks in the El Altar zone of the Maimón Formation include breccias and conglomerates along with well laminated fine-grained meta-tuffs, dark graphite-shales (Fig. 3e), cherts and limestones.

5. Bulk composition and mineral assemblages

Previous to metamorphism, the oceanic volcanic rocks of the Maimón Formation underwent seafloor metamorphism (forming keratophyres and spilites) and an intense hydrothermal alteration associated with the formation of volcanogenic massive sulfide mineralization (Torró et al., 2016). The latter involved silicification, propylitization, sericitization and sulfiditization of the hosting rocks, which were much more intense in the footwall of the massive lenses than in the hanging wall rocks. Compared to major element composition of pristine basalts from the nearby Los Ranchos Formation (which includes island arc tholeiites and boninites; Escuder-Viruete et al., 2006) and the Izu-Bonin-Mariana forearc (which includes forearc basalts and boninites; Reagan et al., 2010), most metabasites from the Maimón Formation are enriched in Al_2O_3 and depleted in CaO (Fig. 4; Table 1). As a result, most Maimón metabasites plot in the field of peraluminous rocks whereas basalts from the Los Ranchos Formation and IBM forearc, as expected, lie in the metaluminous field (Fig. 4a). Although most plagiorhyolites from the Los Ranchos Formation and IBM forearc (data of Reagan et al., 2008) are only weakly peraluminous, metaplagiorhyolites from Maimón are strongly peraluminous. The strong mobilization of elements is further evidenced in the chemographic diagram of Fig. 4b, in which bulk compositions of basalts from the Los Ranchos Formation are compatible with magmatic phases (olivine, orto- and clino-pyroxene and plagioclase), as described by Escuder-Viruete et al. (2006), whereas most Maimón metabasites are not. Instead, the latter are compatible with a hydrothermal alteration assemblage formed by muscovite (sericite), albite-epidote-chlorite (propylitic alteration) and quartz ascribed to the formation of volcanogenic massive sulfide mineralization (e.g., Galley et al., 2007).

The generalized major element mobility due to seafloor metamorphism and hydrothermal alteration processes, added to the initial diversity of the lavas, conferred a marked pre-metamorphic geochemical heterogeneity to the Maimón protoliths. Major element composition of the protoliths determined the metamorphic mineral assemblages and hence studied rocks are grouped into 7 groups described separately below based on chemographic diagrams (Fig. 5). Discrimination of mafic (basalts and basaltic andesites) from felsic (rhyodacites) protoliths was carried out on the basis of immobile elements (HFSE, REE and transition metals) in Torró et al. (2016, in press).

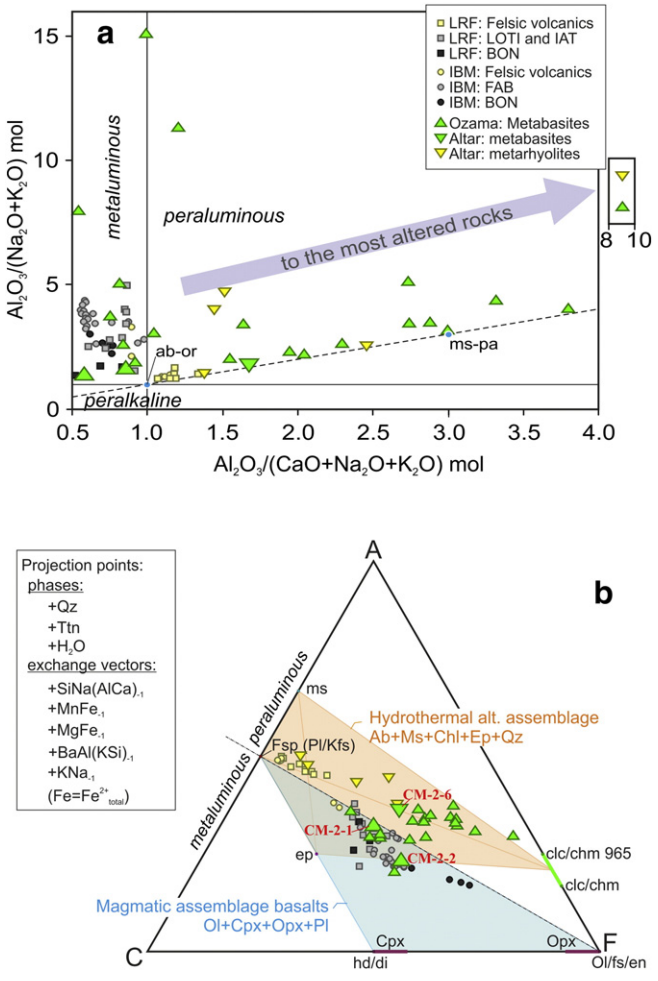

Fig. 4. Plot of whole rock geochemical data of studied Maimón samples in (a) the A/CNK [= molar ratio of $Al_2O_3/(CaO + Na_2O + K_2O)$] vs A/NK [= molar ratio of $Al_2O_3/(Na_2O + K_2O)$] diagram after Shand (1943) and (b) the ACF diagram after projection from Qz, Ttn and H_2O and along the indicated exchange vectors. In b), the likely magmatic assemblage of the mafic protoliths is given on the basis of petrography of unaltered basaltic rocks of the lower basaltic unit of the Los Ranchos Formation according to Escuder-Viruete et al. (2006); the represented hydrothermal assemblage includes mineral phases associated with formation of volcanogenic magmatic sulfide mineralization worldwide. Plots include data of boninites (BON), IAT and low-Ti IAT (LOTI) basalts and felsic volcanic rocks of the Los Ranchos Formation (LRF; Escuder-Viruete et al., 2006), boninites and forearc basalts (FAB) from the Izu-Bonin-Mariana (IBM) forearc (Reagan et al., 2010) and felsic volcanic rocks from Saipan-Rota, Mariana Islands (Reagan et al., 2008) for comparison. Larger symbols represent samples used for thermobarimetric constraints.

5.1. Metabasites of the Ozama shear zone

In the Ozama shear zone, mafic meta-volcanic rocks are prevalent. Torró et al. (2016, in press) determined, on the basis of immobile elements, that the basaltic suite included boninites and low-Ti tholeiites. According to metamorphic assemblages (and defining major element bulk rock compositions) these rocks are grouped into three main groups herein (Fig. 5a–b).

Group O1 lithotype comprises metabasites with bulk compositions typical of pristine island arc basalts (including tholeiites and boninites) in terms of major elements (e.g., samples CM-2-1 and CM-2-2). These rocks have the lowest Al_2O_3 values among the studied basalts, Mg# varies from 58 to 63, and CaO > Na_2O and ≫K_2O. The metamorphic assemblage is composed of amphibole-chlorite-epidote-albite, along with less abundant quartz and phengite. In the ACF and AFM diagrams of Fig. 5a–b, Group O1 basalts match the compositions of unaltered boninites from the Los Ranchos Formation (Escuder-Viruete et al., 2006) and from the Marianas forearc (Reagan et al., 2010), and have characteristic lower C (i.e., CaO) and higher F ($FeO^* + MgO + MnO$) than most unaltered forearc basalts from Marianas forearc and tholeiites from the Los Ranchos Formation.

Group O2 lithotype comprises metabasites (e.g., CM-30 and CM-31) enriched in Al_2O_3 to pristine basalts, and have Mg# between 50 and 58. Calcium is enriched relative to Group O1 and CaO > ($Na_2O + K_2O$). Metamorphic assemblage in these rocks is composed of dominant chlorite-epidote-albite-phengite-quartz, lacking amphibole. In the ACF and AFM diagrams of Fig. 5a–b, A (Al_2O_3) is enriched relative to most boninites and forearc basalts from the Marianas forearc and is similar to the bulk of island arc tholeiites (including basalts to andesites) of the Los Ranchos Formation.

Group O3 lithotype has characteristic very low CaO (<2.8 wt.%) values, lower than Na_2O and similar to K_2O; Al_2O_3 contents are comparable to Group O2, and Mg# has a wide range between 50 and 70 (e.g., CM-26, CM-2-10 and CM-2-12). Chlorite, phengite and albite are the dominant metamorphic phases along with minor epidote and quartz. In the ACF diagram (Fig. 5a), these rocks clearly differentiate of basalts from the Los Ranchos Formation and the Marianas forearc. Inasmuch as Group O3 rocks classify as basalts (Torró et al., 2016, in press), this set stands out for the most hydrothermally altered basalts previously to metamorphism.

Table 1
Major element chemical composition of metavolcanic rocks of the Ozama and the El Altar zones of the Maimón Formation. See Torró et al. (accepted) for analytical methods and precision estimates.

Region	Maimón Ozama																		Maimón Altar				
Roca	Metabasite																		Metabasite	Metapelite			
Group	O1	O1	O1	O1	O2	O2	O2	O3	O3	O3	O3	O3	O3	O3	O3	O3	O3	O3	A1	A2	A3	A4	A4
Rock sample	CM-2-1	CM-2-2	GII-2-3	CM-390-10	CM-30	CM-31	GII-2-4	CM-26	CM-2-3	CM-2-10	CM-2-12	CM-390-14	CM-305-10	CM-344	CM-344	CM-344	CM-305-06	CM-393-7	CM-2-6	CM-15	CM-24	CM-16	CM-2-7
SiO_2 (wt.%)	55.07	57.02	56.33	45.92	54.99	49.70	58.14	63.34	54.72	58.16	64.88	57.27	59.37	58.36	60.63	58.33	58.18	57.01	59.81	72.73	76.93	61.48	71.88
TiO_2	1.03	0.28	0.40	0.30	0.54	0.53	0.43	0.64	0.61	0.60	0.80	0.51	0.62	0.58	0.48	0.41	0.64	0.65	0.48	0.40	0.35	0.56	0.27
Al_2O_3	15.39	10.61	15.47	12.91	15.61	17.88	14.46	14.46	16.62	15.78	13.49	16.23	15.68	16.14	14.98	16.02	14.72	14.83	16.06	14.90	11.35	16.25	12.45
FeO(t)[a]	8.68	9.13	7.47	7.10	8.54	9.20	6.97	8.25	9.10	8.16	7.98	8.04	8.90	8.64	6.59	6.78	10.06	10.08	7.47	2.35	2.81	6.05	2.03
MnO	0.18	0.21	0.15	0.31	0.16	0.15	0.10	0.16	0.21	0.19	0.11	0.18	0.14	0.17	0.18	0.21	0.25	0.43	0.21	0.03	0.22	0.06	0.10
MgO	5.49	8.79	6.06	8.34	5.16	7.10	4.58	4.63	7.13	6.92	4.38	6.57	6.79	6.55	8.58	8.92	7.42	8.49	5.69	0.41	2.66	4.03	2.26
CaO	4.57	5.72	6.82	12.25	8.10	7.30	8.43	0.11	1.31	0.69	0.20	2.82	0.13	1.50	0.60	0.50	0.58	0.17	0.54	0.35	0.13	4.03	3.05
SrO	0.01	0.00	0.03	0.03	0.01	0.01	0.02	0.00	0.00	0.00	0.00	0.01	0.00	0.01	0.00	0.00	0.00	0.00	0.00	0.00	0.00	0.04	0.00
BaO	0.00	0.01	0.02	0.00	0.00	0.01	0.01	0.02	0.00	0.00	0.02	0.00	0.00	0.01	0.00	0.00	0.00	0.02	0.00	0.01	0.01	0.02	0.02
Na_2O	5.84	4.18	3.37	0.92	0.53	0.83	1.71	1.54	5.05	4.17	3.44	2.87	3.04	1.18	2.64	2.79	2.01	0.00	5.22	5.26	2.47	0.63	0.59
K_2O	0.05	0.94	0.47	0.10	0.15	0.20	1.02	0.99	0.05	0.01	0.54	0.06	0.00	1.14	0.03	0.06	0.07	1.34	0.02	1.40	0.30	2.20	1.95
LOI	2.23	1.74	2.18	10.28	4.78	5.47	2.62	4.22	3.77	3.88	2.83	3.72	3.72	4.14	4.39	4.37	4.19	5.62	3.36	1.29	1.95	3.30	4.74
Total	98.70	98.83	98.88	98.58	98.64	98.46	98.59	98.49	98.68	98.68	98.77	98.37	98.48	98.53	99.24	98.60	98.25	98.80	98.96	99.20	99.25	98.75	99.41
SiO_2 (at. %)	60.44	59.90	61.19	53.09	61.88	56.60	63.83	71.52	60.98	64.61	71.58	63.82	66.07	65.62	66.26	64.44	64.88	64.22	66.30	80.11	82.61	69.11	80.16
TiO_2	0.85	0.22	0.33	0.26	0.46	0.45	0.35	0.54	0.51	0.50	0.66	0.43	0.52	0.49	0.39	0.34	0.54	0.55	0.40	0.33	0.28	0.47	0.23
Al_2O_3	9.95	6.57	9.90	8.80	10.35	12.00	9.35	9.62	10.91	10.33	8.77	10.66	10.28	10.69	9.65	10.43	9.67	9.84	10.49	9.67	7.18	10.76	8.18
FeO	7.97	8.02	6.78	6.86	8.04	8.77	6.40	7.79	8.48	7.58	7.37	7.49	8.28	8.12	6.02	6.27	9.38	9.49	6.93	2.16	2.52	5.68	1.90
MnO	0.17	0.19	0.14	0.30	0.15	0.14	0.10	0.15	0.20	0.17	0.10	0.17	0.13	0.16	0.17	0.20	0.24	0.41	0.20	0.02	0.20	0.06	0.10
ZnO	0.01	0.01	0.00	0.01	0.01	0.00	0.01	0.04	0.01	0.02	0.02	0.00	0.01	0.01	0.01	0.01	0.03	0.05	0.01	0.00	0.01	0.01	0.01
MgO	8.98	13.76	9.81	14.37	8.66	12.05	7.50	7.79	11.85	11.46	7.20	10.91	11.26	10.98	13.98	14.69	12.34	14.26	9.40	0.67	4.26	6.75	3.76
CaO	5.37	6.44	7.94	15.17	9.77	8.91	9.92	0.13	1.56	0.82	0.24	3.37	0.16	1.81	0.70	0.59	0.69	0.21	0.64	0.41	0.15	4.85	3.64
SrO	0.00	0.00	0.02	0.02	0.01	0.00	0.01	0.00	0.00	0.00	0.00	0.01	0.00	0.01	0.00	0.00	0.00	0.00	0.00	0.00	0.00	0.02	0.00
BaO	0.00	0.00	0.01	0.00	0.00	0.00	0.00	0.01	0.00	0.00	0.01	0.00	0.00	0.01	0.00	0.00	0.00	0.01	0.00	0.00	0.00	0.01	0.01
Na_2O	6.21	4.26	3.55	1.03	0.58	0.92	1.82	1.69	5.46	4.49	3.68	3.10	3.28	1.29	2.80	2.99	2.17	0.00	5.61	5.62	2.57	0.69	0.64
K_2O	0.04	0.63	0.33	0.07	0.11	0.15	0.71	0.71	0.04	0.01	0.38	0.04	0.00	0.82	0.02	0.04	0.05	0.96	0.01	0.98	0.21	1.58	1.39

[a] Total Fe expressed as FeO.

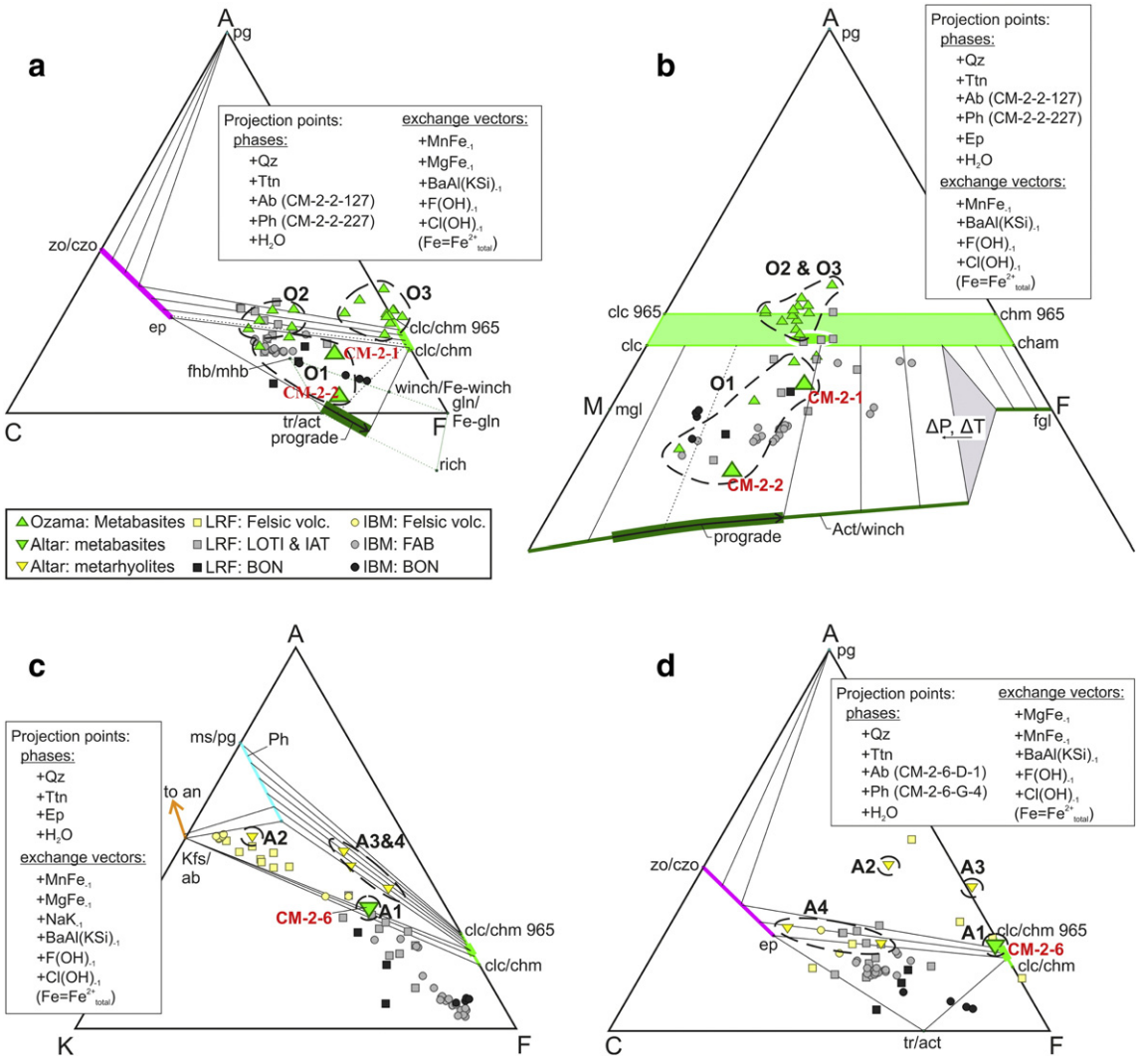

Fig. 5. ACF, AFM and AKF plots for whole rock data of volcanic samples from the Ozama shear zone (a, b) and the El Altar zone (c, d) of the Maimón Formation. Mineral phases observed in the metamorphic assemblages of the studied rocks from each zone are represented schematically (see Fig. 12 for details). Projection points and exchange vectors are indicated for each diagram. For chlorite, chm 965 and clc 965 refer to chamosite and clinochlore with atomic abundances of Fe-Mg, Al and Si of 9, 6 and 5 (per 10 O and 8 OH), respectively (Spear, 1993). Only bulk composition of rocks used for thermobarimetric calculations are labeled.

5.2. Metabasites and metaplagiorhyolites of the El Altar zone

In the El Altar zone, felsic meta-volcanic rocks are, by far, prevalent over mafic ones. Group A1 is defined by the analyzed metabasite sample (CM-2-6). Group A1 metabasite has similar major element composition equivalent to Group O3, and hence is representative of hydrothermally altered basalts. The metamorphic mineral assemblage is defined by dominant chlorite-albite-quartz, less abundant phengite and epidote and trace paragonite (Fig. 5c–d).

According to major element bulk rock compositions and metamorphic assemblages, felsic meta-volcanic rocks from the el Altar zone are grouped into three main groups.

Group A2 comprises a metaplagiorhyolite sample (CM-15) with $Na_2O > K_2O$ and $\gg CaO$. Its metamorphic assemblage is composed of albite, phengite, paragonite, quartz, epidote and minor chlorite. In the AKF diagram of Fig. 5c, its composition matches that of felsic volcanics from the Los Ranchos Formation (Escuder-Viruete et al., 2006) and IBM (Reagan et al., 2008), whereas its depletion in CaO relative to these rocks is evident in the ACF diagram of Fig. 5d.

Group A3 comprises a metaplagiorhyolite sample (CM-24) with $Na_2O \gg K_2O$ and CaO. Its metamorphic assemblage is composed of phengite, chlorite, paragonite, quartz and trace epidote and preserves scarce phenocrysts of albite and quartz. Its depletion in K_2O and CaO relative to unaltered felsic volcanics from the Los Ranchos Formation and IBM is evident in the AKF and ACF diagrams (Fig. 5c–d).

Group A4 is composed of two metaplagiorhyolites (CM-16 and CM-2-7) with $CaO > K_2O$ and $\gg Na_2O$. Their metamorphic assemblage is composed of phengite chlorite, quartz and epidote. In the AKF diagram in Fig. 5c, K (i.e., K_2O and Na_2O) is clearly depleted relative to felsic volcanics from Los Ranchos and IBM, whereas CaO contents are broadly equivalent (Fig. 5d).

6. Mineral chemistry

6.1. Amphibole

This mineral is present only in rocks of the Group O1 of the Ozama shear zone and occurs as zoned, folded crystals along compositional layers interspersed with albite (Fig. 6). Amphiboles belong to the calcium and sodium-calcium subgroups (Fig. 7a) according with the classification scheme of Hawthorne et al. (2012). Analyses yielded very low Ti (<0.05 a.p.f.u.), Mn (<0.06) and K (<0.16) concentrations, and the contents of F (<0.07) and Cl (<0.05) are almost negligible.

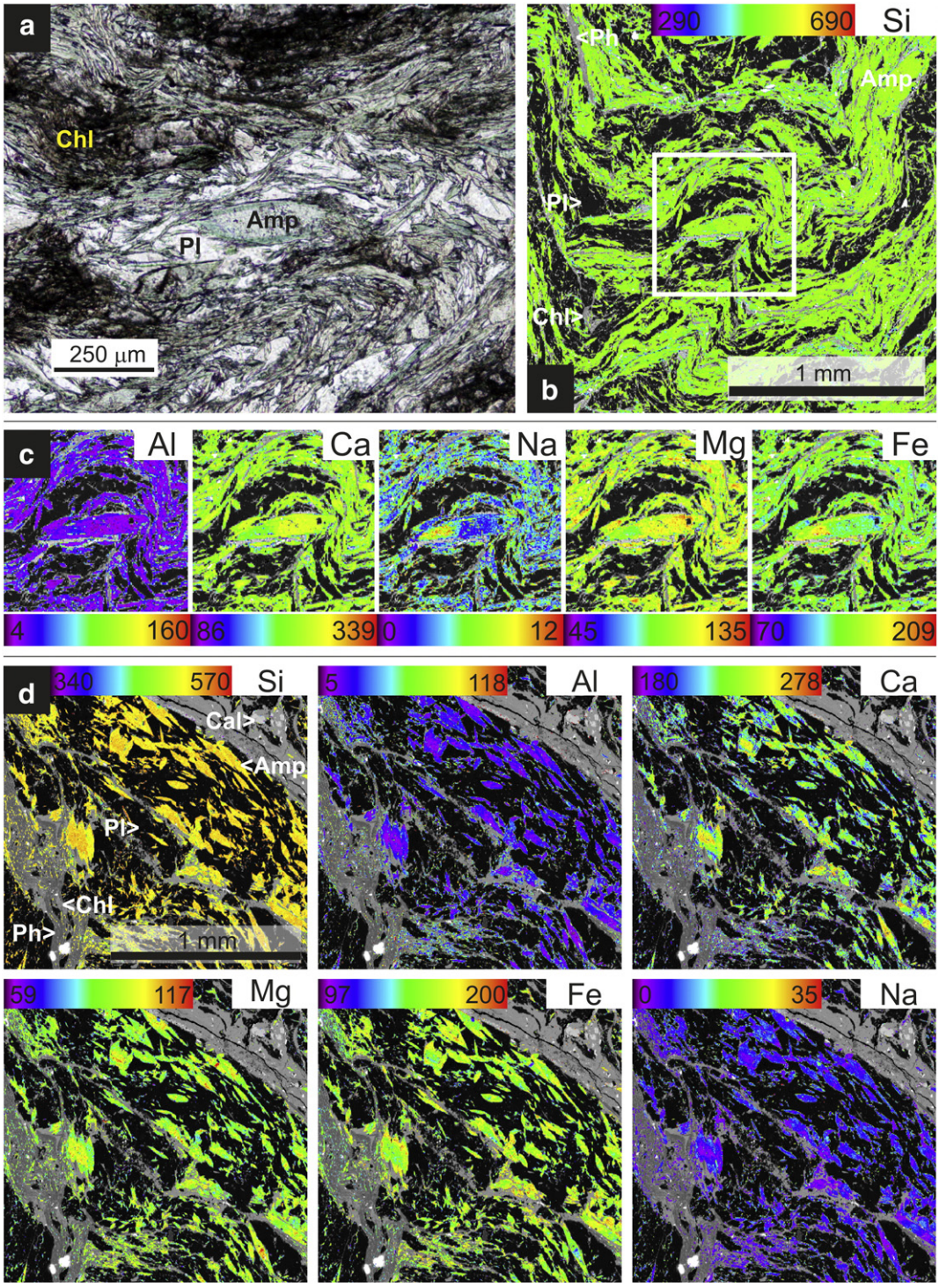

Fig. 6. Photomicrographs (a) and X-ray images (b–d) of amphibole-rich domains in greenschist rocks from the Ozama shear zone. (a) Detail of a zoned amphibole crystal (center of the image) and partially folded amphibole lepidoblasts describing polygonal arcs (optical microscope, plain polarized transmitted light). (b) X-ray image of Si in amphiboles; note the occurrence of both, deformation (folding) of amphibole lepidoblasts and local polygonal arcs defined by tabular amphibole crystals. (c) Aluminum, Ca, Na, Mg and Fe X-ray images of a non-folded zoned amphibole crystal; scanned area in (b). (d) Silicon, Al, Ca, Mg, Fe, Na X-ray images showing textures and zoning of amphibole crystals. In X-ray images (b–d), other mineral phases are masked out and the resulting images are overlain onto a gray-scale BSE image. Color scale bar represents the relative element concentration in counts.

Calcium amphiboles (Ca_B = 1.50–1.91 a.p.f.u.; Na_B = 0.01–0.40) classify as actinolite and very seldom magnesio-ferri-hornblende, with a continuous compositional spectrum between the two species (Fig. 7c–d; Table 2). Calcium amphiboles have variable Si (7.46–7.99 a.p.f.u.), Al_{tot} (0.09–0.73), Mg (2.73–3.77), Fe_{tot} (1.13–2.11), Ca (1.50–1.91) and Na (0.07–0.66) contents. The vacancy in position A is of 0.67 to 1.00 p.f.u. Calculated Fe^{3+} is <0.39 a.p.f.u. Mg# ranges from 0.60 to 0.78.

Sodium-calcium amphiboles (Ca_B between 1.17 and 1.38 a.p.f.u.; Na_B between 0.53 and 0.71) classify as ferri-winchite (Fig. 7b; Table 2). Ferri-winchite crystals yielded relatively homogeneous Si (7.81–7.87 a.p.f.u.), Al_{tot} (0.35–0.46) and Fe_{tot} (1.93–2.11), and

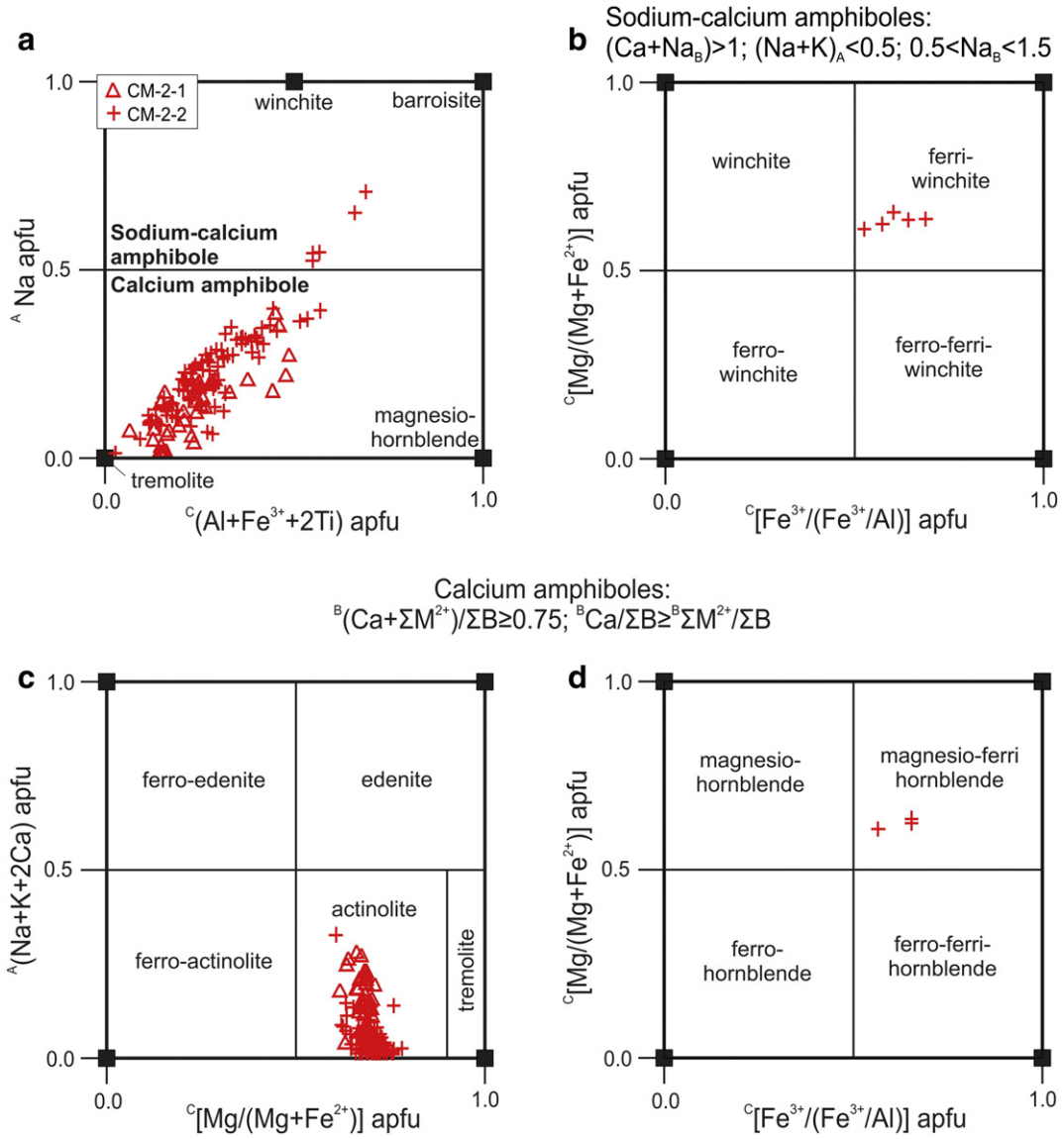

Fig. 7. Composition of calcium and sodium-calcium amphiboles from the Ozama shear zone plotted in the classification scheme of Hawthorne et al. (2012). In (a), filled black squares are the locations of named Mg end-members. Analyzed sodium-calcium amphiboles are represented in (b), and calcium amphiboles in (c) and (d).

antipathetic values of Ca (1.17–1.38) and Na (0.63–0.88). The vacancy in position A ranges from 1.83 to 1.90 p.f.u. Calculated Fe^{3+} is <0.44 and Mg# ranges between 0.60 and 0.65.

Amphibole crystals show marked compositional, roughly concentric, zoning in terms of Si, Al, Mg, Fe, Ca and Na (Fig. 6). Changes in Si, Mg and Ca are inversely compensated by changes in the Al, Fe and Na content, therefore following the cationic exchange between actinolite and ferri-winchite end-members. The ferri-winchite compositions appear at the rim of actinolite grains (Fig. 6c–d).

6.2. White micas (phengite and paragonite)

White mica occurs in most rocks from both the Ozama and El Altar zones; it is, in general, very fine grained (<1 μm wide), which prevented the appropriated chemical analysis in most samples. White micas classify as phengite and paragonite. Phengite is broadly submicroscopically intergrown with chlorite, and in rocks of groups A2 and A3 of the El Altar zone, in addition, is intergrown with paragonite (Fig. 8). Hence, most EMP analyses of white mica in rocks from the El Altar zone represent mixed analysis of phengite-paragonite. In rocks of the Ozama shear zone, systematic variations in the chemical composition of phengites from S_{p-1} and S_p foliations were not observed as a consequence of rotation (by means of crenulation and shear deformation) of S_{p-1} grains into Sp.

The analyzed white mica (phengite and paragonite) lepidoblasts from the Maimón Formation display a continuous relatively wide compositional spectrum (Table 3; Figs. 9 and 10). Remarkably high Si contents (3.16–3.54 a.p.f.u.) of phengite grains from the Ozama shear zone are distinctive to those from the El Altar zone (3.01–3.27). Phengite grains from the Ozama shear zone are richer in Mg (0.13–0.51) and Fe (0.12–0.54) relative to those from the el Altar zone (0.03–0.37 and 0.02–0.20, respectively). Phengite records an increase in ^{iv}Al (0.46–0.84) and ^{vi}Al (1.19–1.80) from the Ozama shear zone to the El Altar zone (0.73–0.99 and 1.65–2.03, respectively). Titanium contents are steadily low (below detection limit) in grains from el Altar, and up to 0.1 a.p.f.u. in samples from the Ozama shear zone. In general, grains from the Ozama shear zone present higher K (0.78–0.97) and lower Na (to 0.05) concentrations than those from el Altar (0.22–0.92 and to 0.52, respectively). Fluorine is up to 0.24 and Cl is systematically under its detection limit.

Table 2
Representative EMP analyses of amphibole from the Ozama and El Altar zones of the Maimón Formation. Cations normalized to 22 O and 2 OH.

Rock sample	CM-2-2	CM-2-2	CM-2-2	CM-2-2	CM-2-2	CM-2-2	CM-2-2	CM-2-2	CM-2-2	CM-2-2	CM-2-1	CM-2-2	CM-2-2	CM-2-2	CM-2-2
Analys. no.	a-2	e-1	e-2	b-5	72.00	74.00	177.00	179.00	180.00	185.00	A 34	a-3	b-3	35.00	211.00
SiO_2	56.64	55.65	56.40	55.75	56.11	56.23	56.37	55.74	56.02	56.04	54.72	52.40	54.29	54.95	54.82
TiO_2	0.02	0.04	d.l.	d.l.	0.05	d.l.	0.03	0.01	0.02	0.07	0.04	0.02	0.07	d.l.	d.l.
Al_2O_3	0.65	0.55	0.68	1.19	1.00	1.04	0.89	1.27	0.78	1.23	1.51	3.29	2.23	2.07	2.13
FeO[a]	10.02	11.68	9.88	11.14	11.07	10.34	11.78	13.31	11.12	8.97	12.02	14.22	13.83	13.32	14.43
Fe_2O_3[a]	0.41	0.43	0.66	1.19	0.83	0.50	0.61	0.59	0.72	0.71	1.48	3.37	4.10	3.07	2.91
MnO	0.26	0.33	0.34	0.33	0.29	0.32	0.28	0.38	0.31	0.23	0.34	0.36	0.34	0.30	0.32
MgO	17.47	16.52	17.34	16.60	16.56	17.22	16.13	14.83	16.23	17.90	15.67	12.73	12.88	13.66	12.98
CaO	12.31	12.48	12.00	11.56	11.73	11.78	11.56	11.00	11.55	12.37	11.94	9.62	7.90	8.86	8.94
Na_2O	0.53	0.24	0.67	0.73	0.76	0.59	0.84	0.99	0.80	0.49	0.62	2.03	2.94	2.43	2.26
K_2O	d.l.	d.l.	d.l.	d.l.	d.l.	d.l.	d.l.	d.l.	d.l.	0.01	0.04	0.07	d.l.	d.l.	d.l.
F	d.l.	d.l.	d.l.	d.l.	d.l.	d.l.	d.l.	d.l.	d.l.	d.l.	d.l.	d.l.	d.l.	d.l.	d.l.
Cl	0.01	d.l.	d.l.	d.l.	0.02	d.l.	0.02	d.l.	0.02	0.01	d.l.	0.01	0.02	d.l.	d.l.
H_2O[b]	2.13	2.10	2.12	2.12	2.11	2.12	2.11	2.10	2.10	2.13	2.10	2.06	2.08	2.09	2.09
Sum	100.47	100.02	100.20	100.61	100.53	100.18	100.65	100.21	99.67	100.15	100.48	100.17	100.67	100.75	100.88
Total[c]	100.47	100.02	100.20	100.61	100.52	100.18	100.65	100.21	99.66	100.15	100.48	100.17	100.67	100.75	100.88
Si	7.98	7.95	7.97	7.90	7.94	7.95	7.98	7.98	7.99	7.89	7.82	7.63	7.82	7.87	7.87
Al(iv)	0.02	0.05	0.03	0.10	0.06	0.05	0.02	0.02	0.01	0.11	0.18	0.37	0.18	0.13	0.13
Al(C)	0.09	0.04	0.09	0.10	0.11	0.12	0.13	0.19	0.13	0.10	0.07	0.20	0.20	0.22	0.23
Ti(C)	0.00	0.00	–	–	0.01	–	0.00	0.00	0.00	0.01	0.00	0.00	0.01	–	–
Fe^{3+}(C)	0.04	0.05	0.07	0.13	0.09	0.05	0.06	0.06	0.08	0.07	0.16	0.37	0.44	0.33	0.31
Mg(C)	3.67	3.52	3.65	3.51	3.49	3.63	3.41	3.16	3.45	3.76	3.34	2.76	2.77	2.92	2.78
Fe^{2+}(C)	1.18	1.39	1.17	1.27	1.30	1.19	1.39	1.58	1.33	1.06	1.43	1.67	1.58	1.54	1.67
Mn(C)	0.02	0.00	0.02	0.00	0.00	0.00	0.00	0.00	0.02	0.00	0.00	0.00	0.00	0.00	0.00
Fe^{2+}(B)	0.00	0.00	0.00	0.05	0.01	0.03	0.00	0.01	0.00	0.00	0.01	0.06	0.09	0.06	0.06
Mn(B)	0.01	0.04	0.02	0.04	0.04	0.04	0.03	0.05	0.02	0.02	0.04	0.04	0.04	0.04	0.04
Ca(B)	1.86	1.91	1.82	1.75	1.78	1.78	1.75	1.69	1.77	1.87	1.83	1.50	1.22	1.36	1.38
Na(B)	0.13	0.05	0.16	0.16	0.18	0.15	0.21	0.25	0.21	0.11	0.12	0.39	0.65	0.55	0.53
Na(A)	0.01	0.02	0.02	0.04	0.03	0.02	0.02	0.02	0.01	0.02	0.05	0.18	0.17	0.13	0.10
K(A)	–	–	–	–	–	–	–	–	–	0.00	0.01	0.01	–	–	–
Vac(A)	0.99	0.98	0.98	0.96	0.97	0.98	0.98	0.98	0.99	0.97	0.94	0.81	0.83	0.87	0.90
OH	2.00	2.00	2.00	2.00	1.99	2.00	1.99	2.00	1.99	2.00	2.00	2.00	1.99	2.00	2.00
F	–	–	–	–	–	–	–	–	–	–	–	–	–	–	–
Cl	–	–	–	–	0.01	–	0.01	–	0.01	0.00	–	0.00	0.01	–	–
Subgroup	Calcium amphiboles												Sodium-calcium amphiboles		
Name	Act	Act	Act	Act	Act	Act	Act	Act	Act	Act	Act	Ferri-mhb	Ferri-win	Ferri-win	Ferri-win

[a] FeO and Fe_2O_3 wt.% concentrations were calculated for electroneutrality.
[b] H_2O wt.% concentration was calculated on the basis of 2 OH p.f.u.
[c] Sum - oxygen equivalent to F and Cl.

Phengite exhibits a marked Tschermak ($Si(Mg,Fe)Al_{-2}$) exchange along the dioctahedral mica series, which relates muscovite ($KAl_2AlSi_3O_{10}(OH)_2$) to the celadonite ($K(Mg,Fe)AlSi_4O_{10}(OH)_2$) end-members (Fig. 9). The Tschermak exchange component is extreme in analyzed phengite crystals from the Ozama shear zone whereas those from the el Altar zone approximate the composition of muscovite/paragonite. A slight but progressive increase in the trioctahedral contents occurs as the composition of phengite deviates from the muscovite end-member. This trioctahedral component may be spurious if, at least in part, it is the result of higher Fe^{3+}/Fe^{2+} ratios (normalizing to 22 negative charges with Fe^{3+} unaccounted for results in an overestimation of all cations in the structural formula, thus increasing the calculated octahedral occupancies; e.g., Garcia-Casco et al., 1993). Although a paragonitic (NaK_{-1}) exchange apparently operates in phengite from the El Altar zone (Fig. 10), antipathetically to the Tschermak exchange (as expected; Guidotti, 1984), these values represent mixed analyses of phengite/paragonite to a large extent.

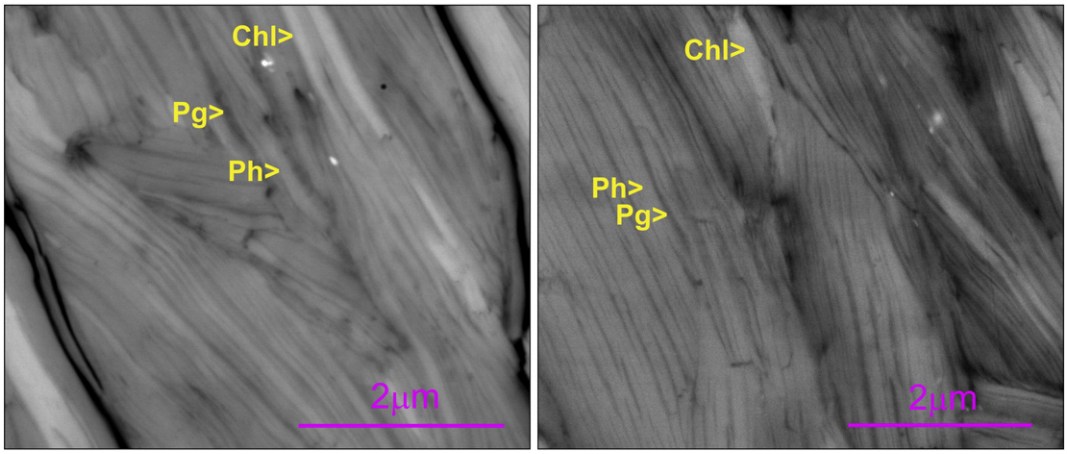

Fig. 8. Detail of the sub-micron scale intergrowths between phengite, paragonite and chlorite in a sample of metaplagiorhyolite from El Altar zone. SEM-BSE image.

Table 3
Representative EMP analyses of phengite from the Ozama and El Altar zones of the Maimón Formation. Cations normalized to 10 O and 2 OH.

	Ozama shear zone									El Altar zone[a]					
Rock sample	CM-26	CM-35	CM-2-12	CM-2-12	CM-2-12	CM-2-2	CM-2-2	CM-2-2	CM-2-2	CM-16	CM-24	CM-24	CM-24	CM-2-6	CM-2-7
Analys. no.	d-12	d-3	A-3	C 14	D 2	A 25	B 137	B 141	C 231	b-3	a-6	d-2	a-1	G-5	D 2
SiO_2	48.70	48.98	47.90	48.44	48.62	51.08	50.86	51.02	50.87	48.31	48.36	47.66	47.46	49.93	49.48
TiO_2	0.04	0.08	0.27	0.25	0.15	0.10	0.14	0.15	0.11	0.01	0.05	0.04	d.l.	0.07	0.03
Al_2O_3	32.57	26.84	27.67	27.46	27.53	24.03	23.37	22.79	20.34	31.00	39.00	38.11	38.42	28.19	35.89
FeO(t)[b]	2.46	5.22	5.08	5.16	4.86	5.97	6.31	6.62	7.97	2.25	0.78	0.87	0.85	5.12	1.81
MgO	1.36	2.47	2.38	2.31	2.60	3.41	3.38	3.61	4.92	2.11	0.41	0.38	0.42	3.24	0.63
Na_2O	0.31	0.08	0.08	0.07	0.11	0.09	0.08	0.07	0.10	0.15	3.57	3.28	8.04	0.80	1.35
K_2O	9.25	10.81	9.95	10.58	10.40	10.78	10.65	10.30	9.07	10.70	3.67	4.36	0.09	6.82	7.37
F	d.l.	d.l.	d.l.	0.14	d.l.	–	–	–	–	0.18	0.47	1.23	d.l.	d.l.	d.l.
Cl	d.l.	d.l.	d.l.	d.l.	d.l.	d.l.	d.l.	d.l.	d.l.	d.l.	d.l.	d.l.	d.l.	d.l.	d.l.
H_2O[c]	4.50	4.36	4.34	4.30	4.38	4.41	4.37	4.36	4.32	4.37	4.49	4.05	4.69	4.48	4.58
Sum	99.21	98.88	97.69	98.74	98.67	100.03	99.20	99.17	98.67	99.23	100.89	100.02	99.97	99.06	101.33
Total[d]	99.21	98.87	97.68	98.68	98.67	100.03	99.20	99.17	98.67	99.15	100.69	99.50	99.97	99.06	101.27
Si	3.24	3.36	3.31	3.32	3.33	3.47	3.49	3.50	3.53	3.25	3.08	3.08	3.03	3.34	3.18
Al(iv)	0.76	0.64	0.69	0.68	0.67	0.53	0.51	0.50	0.47	0.75	0.92	0.92	0.97	0.66	0.82
Al(vi)	1.79	1.52	1.56	1.54	1.54	1.39	1.37	1.35	1.19	1.71	2.00	1.99	1.93	1.57	1.91
Ti	0.00	0.00	0.01	0.01	0.01	0.00	0.01	0.01	0.01	0.00	0.00	0.00	–	0.00	0.00
Fe	0.14	0.30	0.29	0.30	0.28	0.34	0.36	0.38	0.46	0.13	0.04	0.05	0.05	0.29	0.10
Mg	0.13	0.25	0.24	0.24	0.27	0.35	0.35	0.37	0.51	0.21	0.04	0.04	0.04	0.32	0.06
sum vi	2.07	2.08	2.11	2.09	2.10	2.09	2.09	2.11	2.17	2.05	2.09	2.07	2.02	2.19	2.07
Na	0.04	0.01	0.01	0.01	0.01	0.01	0.01	0.01	0.01	0.02	0.44	0.41	0.99	0.10	0.17
K	0.79	0.94	0.88	0.93	0.91	0.93	0.93	0.90	0.80	0.92	0.30	0.36	0.01	0.58	0.61
Vac	0.17	0.04	0.11	0.06	0.08	0.05	0.06	0.08	0.12	0.06	0.26	0.23	0.00	0.30	0.23
sum xii	0.83	0.96	0.89	0.94	0.92	0.95	0.94	0.92	0.88	0.94	0.74	0.77	1.00	0.70	0.77
OH	2.00	1.99	2.00	1.97	2.00	2.00	2.00	2.00	2.00	1.96	1.91	1.75	2.00	2.00	1.97
F	–	–	–	0.03	–	–	–	–	–	0.04	0.09	0.25	–	–	–
Cl	–	–	–	–	–	–	–	–	–	–	–	–	–	–	–

[a] Due to the very fine intergrowths of paragonite and phengite, these values represent mixed compositions.
[b] Total Fe expressed as FeO.
[c] H_2O wt.% concentration was calculated on the basis of 2 OH p.f.u.
[d] Sum - oxygen equivalent to F and Cl.

6.3. Chlorite

Chlorite crystals from the El Altar and Ozama shear zones present higher Mg (2.61–3.01 and 2.21–2.85 a.p.f.u., respectively) than Fe (1.25–2.00 and 1.74–2.38) and Al^{vi} (1.19–1.72 and 0.76–1.64) contents (Table 4). Manganese contents are systematically low (0.02–0.05). Although most of the analyses plot near the fully octahedral occupancy line (Fig. 11a), a chlorite crystals from the Ozama shear zone returned up to 0.29 octahedral vacancies p.f.u. In the tetrahedral position of chlorite from the El Altar and the Ozama shear zones, Si (2.71–2.80 and 2.70–3.14,) broadly doubles and triples, respectively, the content in Al^{iv} (1.20–1.29 and 0.86–1.30). Fluorine and Cl contents are almost negligible. According to these data, the chlorites are tri-trioctahedral and belong to the clinochlore-chamosite series (Wiewióra and Weiss, 1990). Mg# is in the range of 0.57–0.70 in the El Altar and of 0.50 to 0.59 in the Ozama shear zones and hence the studied chlorites classify as clinochlore. The compositional deviation from the clinochlore-chamosite binary can be largely described by the Tschermak exchange ($Si(Mg,Fe)Al_{-2}$) (Fig. 11b).

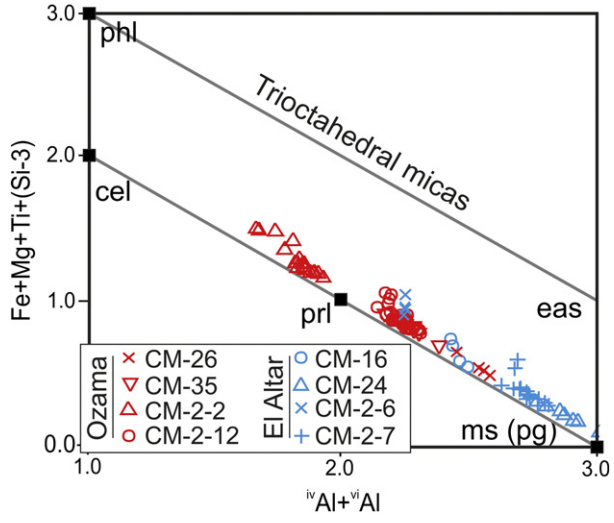

Fig. 9. Multicationic diagram including relevant mica end-members illustrating the continuous nature of the coupled cation substitutions underlying the compositional variation within the investigated phengite crystals from the Maimón Formation.

6.4. Plagioclase

In the Ozama and El Altar zones, plagioclase feldspar is virtually pure albite ($Ab_{96–100}$; Table 5), with very low orthoclase (Or ≤2.27); nevertheless, K is systematically higher in plagioclase crystals from the Ozama shear zone ($Or_{0.24–2.27}$) to those of the El Altar zone ($Or_{0.06–0.13}$).

6.5. Epidote

Epidote group minerals in both the Ozama and the El Altar zones yielded comparable compositions and a very limited compositional range that allows their classification as epidote (sensu stricto; Franz and Liebscher, 2004). The content of Fe^{3+} (0.45–0.66 a.p.f.u.) is remarkably higher than that of Al(M3) (up to 0.29) and Mn (up to 0.02).

7. P–T estimates of metamorphic conditions

Isochemical P–T projection (pseudosection) was calculated for sample CM-2-2, representative of the bulk-rock composition of the Group O1 rocks from the Ozama shear zone. This sample was selected because of its most diverse metamorphic mineral assemblage (i.e., lower variance; Fig. 12), larger mineral grain sizes (suggesting

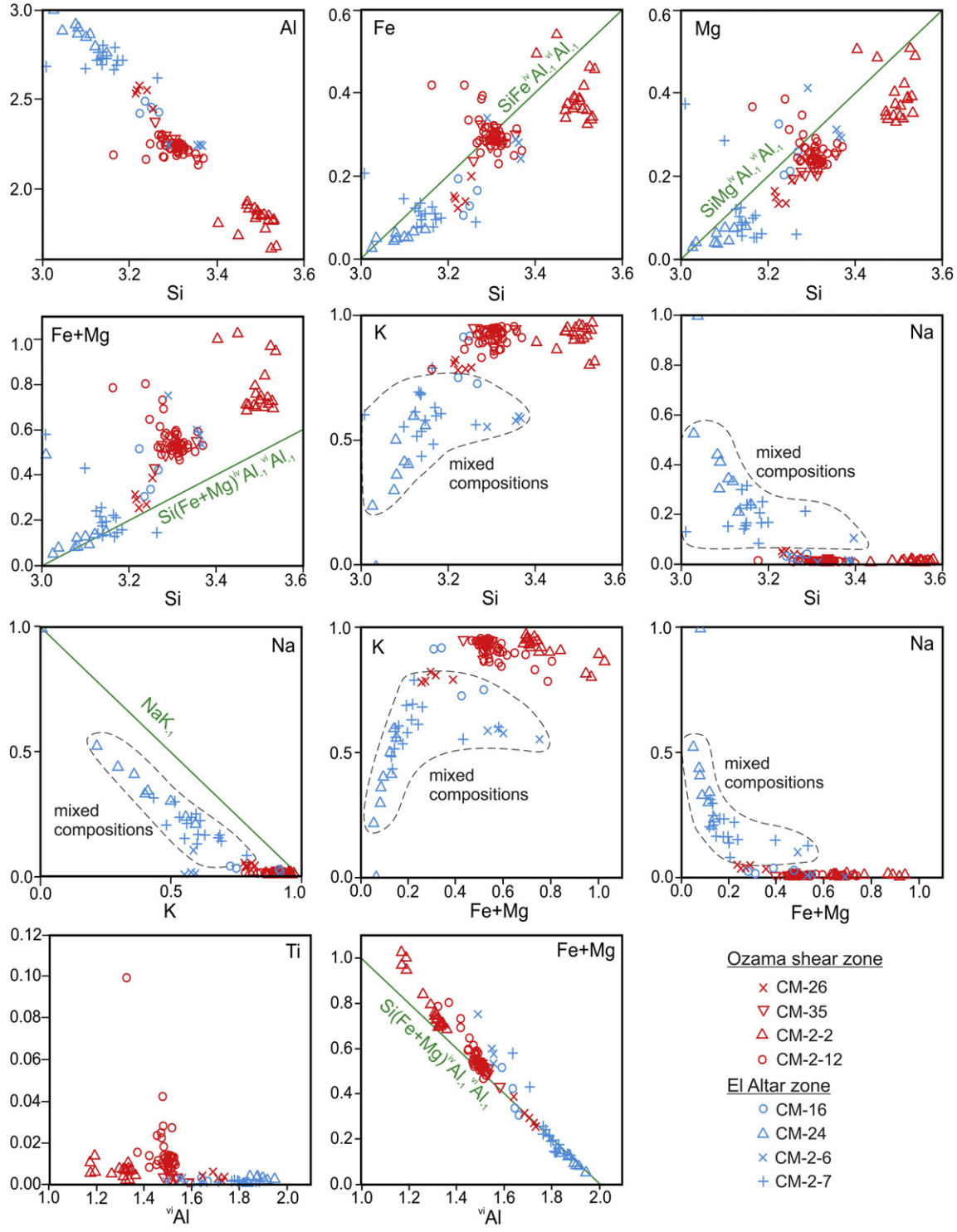

Fig. 10. Selected bivariate diagrams showing the compositional spectrum of the studied phengites from the El Altar and the Ozama zones, Maimón Formation. Mixed analyses in fine phengite + paragonite intergrowths in rocks from the El Altar zone are indicated for the bivariate diagrams involving Na and K.

metamorphic equilibration of the minerals) and presence of ferri-winchite (suggesting higher P–T peak conditions).

The pseudosection for sample CM-2-2 shows a field with the association Ca-Amp + Chl + Ep + Ph + Ab + Qz + Hem consistent with the observed mineral assemblage in the sample (Fig. 13a). Close to and at higher P of this field, Na-Ca-Amp occurs, suggesting that the P–T path crosscut the winchite-in line. To further constrain the P–T conditions, mineral composition isopleths for phengite (Si) and chlorite (Mg#) were calculated (Fig. 13b). The distribution of isopleth confirms the Ca-Amp + Chl + Ep + Ph + Ab + Qz + Hem field and fixes the conditions to ~8.2 kbar and 380 °C. The obtained temperature is also in agreement with the low temperature nature of the quartz CPOs (~350°; Blacic, 1975) from the Ozama shear zone (Draper and Gutiérrez-Alonso, 1997) where they exhibit monoclinic, small circle girdle (SG) fabrics and monoclinic type 1 crossed girdle (CG) fabrics (Lister, 1977; Schmid and Casey, 1986), consistent with a simple shear context and indicate <a> directed basal slip.

Table 4
Representative EMP analyses of chlorite from the Ozama and El Altar zones of the Maimón Formation. Cations normalized to 10 O and 8 OH.

	Ozama shear zone								El Altar zone			
Rock sample	CM-26	CM-2-12	CM-2-1c	CM-2-2	CM-2-2	CM-2-2	CM-2-2	CM-2-2	CM-2-7	CM-2-7	CM-2-7	CM-2-7
Analys. no.	d-9	D 6	A 3	A 31	B 163	B 164	C 235	C 238	C 122	C 124	C 131	D 140
SiO_2	29.46	25.79	27.71	28.91	28.94	26.99	28.39	27.76	29.06	27.83	26.41	28.72
TiO_2	0.04	0.04	d.l.	0.00	0.02	0.00	0.00	0.03	0.00	0.01	0.00	0.00
Al_2O_3	22.24	20.40	18.08	16.91	16.29	18.42	17.55	18.98	24.48	24.18	22.65	25.53
FeO(t)[a]	20.51	26.57	24.45	23.50	25.71	26.11	24.51	25.12	16.23	15.59	16.55	15.34
MnO	0.28	0.33	0.46	0.46	0.40	0.47	0.53	0.52	0.39	0.39	0.39	0.34
MgO	14.62	15.69	18.09	17.99	17.24	16.66	17.35	16.52	20.16	19.98	19.72	18.89
CaO	0.03	d.l.	0.14	0.32	0.11	0.04	0.05	0.05	0.03	0.00	0.04	0.01
Na_2O	0.07	d.l.	d.l.	0.00	0.12	0.00	0.00	0.00	0.03	0.04	0.11	0.03
K_2O	0.64	0.03	d.l.	0.00	0.00	0.00	0.00	0.00	0.03	0.02	0.06	0.22
F	d.l.	0.09	d.l.	–	–	–	–	–	0.15	0.10	0.22	0.13
Cl	d.l.	d.l.	d.l.	d.l.	d.l.	d.l.	d.l.	d.l.	d.l.	d.l.	d.l.	d.l.
H_2O[b]	11.84	11.40	11.59	11.56	11.50	11.45	11.54	11.59	12.39	12.08	11.60	12.28
Sum	99.98	100.35	100.54	99.64	100.41	100.15	99.92	100.56	102.96	100.22	97.75	101.49
Total[c]	99.98	100.31	100.54	99.64	100.39	100.15	99.92	100.56	102.89	100.18	97.66	101.43
Si	2.98	2.70	2.87	3.00	3.01	2.83	2.95	2.87	2.80	2.75	2.71	2.79
Al(iv)	1.02	1.30	1.13	1.00	0.99	1.17	1.05	1.13	1.20	1.25	1.29	1.21
Al(vi)	1.64	1.22	1.07	1.07	1.01	1.10	1.10	1.19	1.57	1.57	1.44	1.72
Ti	0.00	0.00	–	0.00	0.00	0.00	0.00	0.00	0.00	0.00	0.00	0.00
Fe	1.74	2.33	2.11	2.04	2.24	2.29	2.13	2.17	1.31	1.29	1.42	1.25
Mn	0.02	0.03	0.04	0.04	0.04	0.04	0.05	0.05	0.03	0.03	0.03	0.03
Mg	2.21	2.45	2.79	2.78	2.68	2.60	2.69	2.55	2.89	2.94	3.01	2.74
Ca	0.00	–	0.02	0.04	0.01	0.00	0.01	0.01	0.00	0.00	0.00	0.00
Na	0.01	–	–	0.00	0.02	0.00	0.00	0.00	0.00	0.01	0.02	0.01
K	0.08	0.00	–	0.00	0.00	0.00	0.00	0.00	0.00	0.00	0.01	0.03
Sum vi	5.71	6.04	6.03	5.97	6.00	6.04	5.97	5.97	5.82	5.84	5.94	5.76
Vac. Vi	0.29	0.00	0.00	0.03	0.00	-0.04	0.03	0.03	0.18	0.16	0.06	0.24
OH	8.00	7.97	8.00	8.00	7.99	8.00	8.00	8.00	7.95	7.97	7.93	7.96
F	–	0.03	–	–	–	–	–	–	0.04	0.03	0.07	0.04
Cl	–	–	–	–	–	–	–	–	–	–	–	–
Mg#	0.56	0.51	0.57	0.58	0.54	0.53	0.56	0.54	0.69	0.70	0.68	0.69

[a] Total Fe expressed as FeO.
[b] H_2O wt.% concentration was calculated on the basis of 8 OH p.f.u.
[c] Sum - oxygen equivalent to F and Cl.

The aforementioned conditions are representative of low temperature and moderate pressure during metamorphism, in the greenschist to blueschist facies transition (e.g., Liou et al., 2004; Spear, 1993) and suggest that our rocks were dragged down in the lithosphere to approximately ~29 km, which corresponds to an apparent geothermal gradient of 13.2 °C/km, compatible with subduction gradients along the slab-mantle interface.

The construction of a pseudosection from a sample from the El Altar zone was declined from the start since the samples from this zone systematically contain magmatic/hydrothermal remnants suggesting

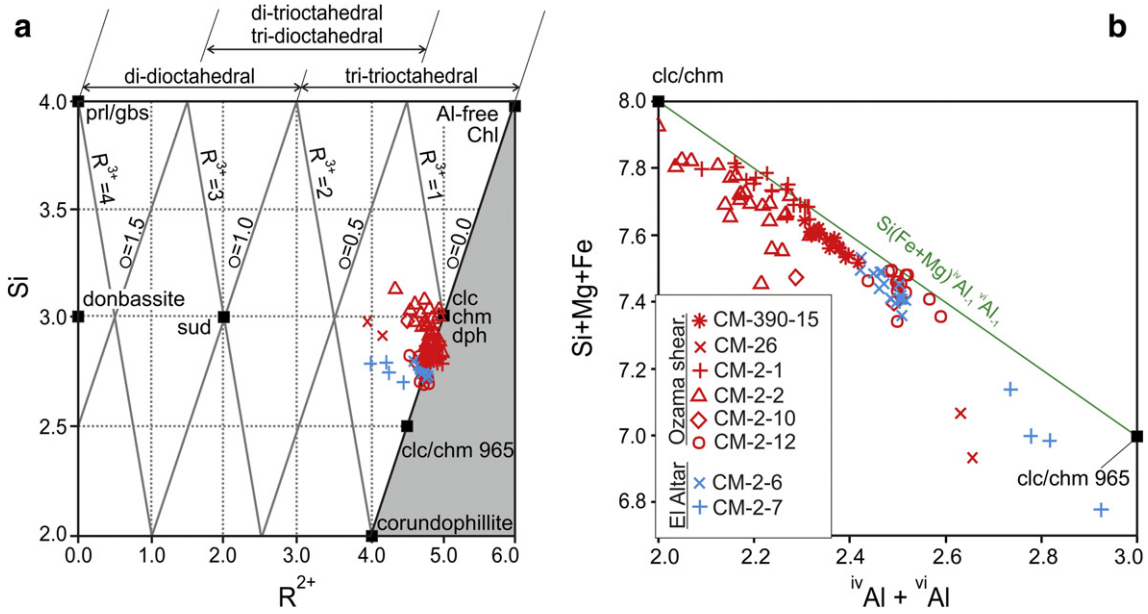

Fig. 11. (a) Multicationic diagram (R^{2+} — Si) for chlorite of the Maimón Formation, including end-members after Wiewióra and Weiss (1990). R^{2+} refers to divalent cations (Fe^{2+}, Mg^{2+} and Mn^{2+}), R^{3+} to trivalent cations (in our case, Al^{3+}) and □ to vacancies. (b) Bivariate Si + Fe + Mg vs. Al(iv) + Al(vi) plot for chlorite from the Maimón Formation.

Table 5
Representative EMP analyses of plagioclase from the Ozama and El Altar zones of the Maimón Formation. Cations normalized to 8 O.

	Ozama shear zone							El Altar zone		
Rock sample	CM-2-2	CM-2-2	CM-2-2	CM-2-2	CM-2-2	CM-2-1c	CM-2-1c	CM-2-6	CM-2-6	CM-2-6
Analys. no.	B 111	B 112	B 126	B 127	B 134	A 239	A 241	17	59	61
SiO_2	67.79	67.95	69.63	69.82	69.71	67.26	67.96	68.38	68.15	68.25
Al_2O_3	18.45	18.38	19.20	19.21	19.31	19.87	19.19	19.46	19.45	19.32
FeO(t)[a]	0.16	0.07	0.16	0.08	0.11	0.04	0.11	0.04	0.06	0.03
CaO	0.09	0.09	0.02	d.l.	d.l.	0.67	0.04	0.09	0.04	0.02
BaO	d.l.	d.l.	0.05	d.l.	0.07	–	–	d.l.	0.02	0.03
Na_2O	11.56	11.62	11.54	12.11	11.96	11.07	11.45	11.90	11.99	11.58
K_2O	0.33	0.41	0.11	0.08	0.06	0.05	0.04	0.02	d.l.	0.02
Total	98.38	98.52	100.71	101.29	101.22	98.96	98.79	99.89	99.70	99.26
Si	3.01	3.02	3.02	3.01	3.01	2.97	3.00	2.99	2.99	3.00
Al	0.97	0.96	0.98	0.98	0.98	1.03	1.00	1.00	1.01	1.00
Fe^{3+}	0.00	0.00	0.00	0.00	0.00	0.00	0.00	0.00	0.00	0.00
Ca	0.00	0.00	0.00	–	–	0.03	0.00	0.00	0.00	0.00
Ba	–	–	0.00	–	0.00	–	–	0.00	0.00	0.00
Na	1.00	1.00	0.97	1.01	1.00	0.95	0.98	1.01	1.02	0.99
K	0.02	0.02	0.01	0.00	0.00	0.00	0.00	0.00	–	0.00
Ca + Ba + Na + K	1.02	1.03	0.98	1.02	1.01	0.98	0.98	1.01	1.02	0.99
%Ab	97.75	97.31	99.30	99.59	99.65	96.48	99.55	99.47	99.77	99.77
%An	0.43	0.42	0.10	–	–	3.25	0.22	0.40	0.17	0.11
%Or	1.81	2.27	0.61	0.41	0.35	0.27	0.24	0.13	0.06	0.13

[a] Total Fe expressed as FeO.

that metamorphic re-equilibration was not completely achieved. In addition, these samples present a conspicuously fine grained nature (including very fine Chl-Ph-Pg intergrowths) that largely prevented the chemical measurement of pure phases, as aforesaid. As a proxy for the estimation of the pressure undergone by rocks of the El Altar zone during metamorphism, we used Si contents of phengite. The tschermak and paragonitic substitutions are known to be strongly influenced by intensive and extensive parameters and to display an antipathetic behavior in muscovite solid solution (cf. Garcia-Casco et al., 1993; Guidotti, 1984). For a given system, a consistent increase in the Si content of phengite occurs with increasing P (and, to a lesser extent, decreasing T). Analyzed phengites from the Maimón Formation have relatively high Si contents, higher in the Ozama shear zone (up to 3.54 a.pf.u) than in the El Altar zone (up to 3.36 a.p.f.u); these values are suggestive of a cold metamorphic gradient during metamorphic recrystallization. Assuming T in the range between 300 and 350 °C, lower than the Ozama zone, the calibrations of the phengite geobarometer by Massonne and Szpurka (1997) and Simpson et al. (2000) yield minimum metamorphic pressure estimates for phengites from the El Altar zone of ~3.5 and 3 kbar, respectively (minimum P of ~6 and 5.5 kbar, respectively, for phengites of the Ozama shear zone). It should be noted that the lack of biotite/phlogopite and K-feldspar in the coexisting assemblages actually makes the calculated pressures to be minimum estimates (Massonne and Schreyer, 1987). In addition, for the El Altar samples, mixed analyses (phengite ± paragonite) may dilute the Si concentration, which would result also in lower P estimates.

8. Discussion

8.1. Metamorphic conditions

Rocks of the Maimón Formation record an inverted metamorphic gradient with a sharp jump in recrystallization at the Fátima thrust fault, which separates the lower grade footwall (i.e., El Altar zone) from the higher grade hanging wall (i.e., Ozama shear zone), where intense syn-metamorphic mylonitic and phyllonitic deformation occurs. Since the early work by Bowin (1960, 1966), the metamorphic assemblage of the Maimón Formation has been considered representative of low-P greenschist facies. This assignation has been recurrently recalled by many authors (Draper and Gutiérrez-Alonso, 1997; Draper and Lewis, 1991; Draper et al., 1996; Escuder-Viruete et al., 2002; Kesler et al., 1991a; Nagle, 1974). Thus, Kesler et al. (1991a) suggested temperatures of about 400 °C and pressures not higher than 3 kbar. On the basis of mineral assemblages in metabasic rocks, Escuder-Viruete et al. (2002) distinguished two metamorphic zones: zone I in the prehnite – pumpellyite facies, with prehnite, pumpellyite, chlorite, epidote, albite, white mica, quartz and calcite; and zone II in the low-pressure greenschist facies, with chlorite, actinolite, epidote, albite, white mica and quartz (in both cases, less than 3 kbar). These authors noted that at least part of the assemblages was pre-kinematic (i.e., pre-tectonic) and produced by spilitization during sea-floor metamorphism. Identical conclusions were reached by Escuder-Viruete et al. (2007b) for the Amina Formation, widely accepted to be a separate segment of the same magmatic and metamorphic belt (i.e., the Maimón-Amina-Tortue Island belt; Draper and Lewis, 1991; Escuder-Viruete et al., 2007b; Kesler et al., 1991a; Lewis and Draper, 1990). Nevertheless, systematic and detailed analyses of minerals and quantitative determinations of pressure and temperature of metamorphism in the Maimón Formation had not hitherto been reported. Only a few analyses of actinolite and albite are given by Escuder-Viruete et al. (2002) in a general study including the Duarte and Río Verde Complexes, and of actinolite in the Amina Formation by Escuder-Viruete et al. (2007b). Paragonite and ferri-winchite have not been reported previously.

Our pseudosection calculations indicate that the high grade rocks of the Ozama shear zone of the Maimón Formation reached peak temperature and pressure of ~8.2 kbar; 380 °C, close to the greenschist to blueschists facies transition (see Fig. 14). Hence, the low-P conditions of metamorphism commonly attributed to the Maimón Formation and the derived tectonic constraints require reconsideration.

The reason why the high metamorphic peak pressures have been unnoticed in previous studies has most probably to do with the hydrothermally modified bulk-rock geochemistry before metamorphism, as discussed above. Peak metamorphic assemblages of studied rocks do not match the mineralogy expected for blueschists (or greenschist/blueschist transition), but rather recall that of greenschist facies bearing abundant epidote, feldspar and chlorite, but scarce amphibole. Only in those few metabasites (the exception) with compositions close to pristine basalts (Group O1), peak ferri-winchite is present (Figs. 5a–b and 12). The rest of metabasites are enriched in Al_2O_3 and, in those most pervasively altered, strongly depleted in CaO and Na_2O relative to pristine basalts; in these compositions, Ca- and Ca-Na- amphiboles do not form (Fig. 5). Glaucophane was not detected in Maimón metabasites in spite of intensive search. In the blueschist facies, Fe-rich

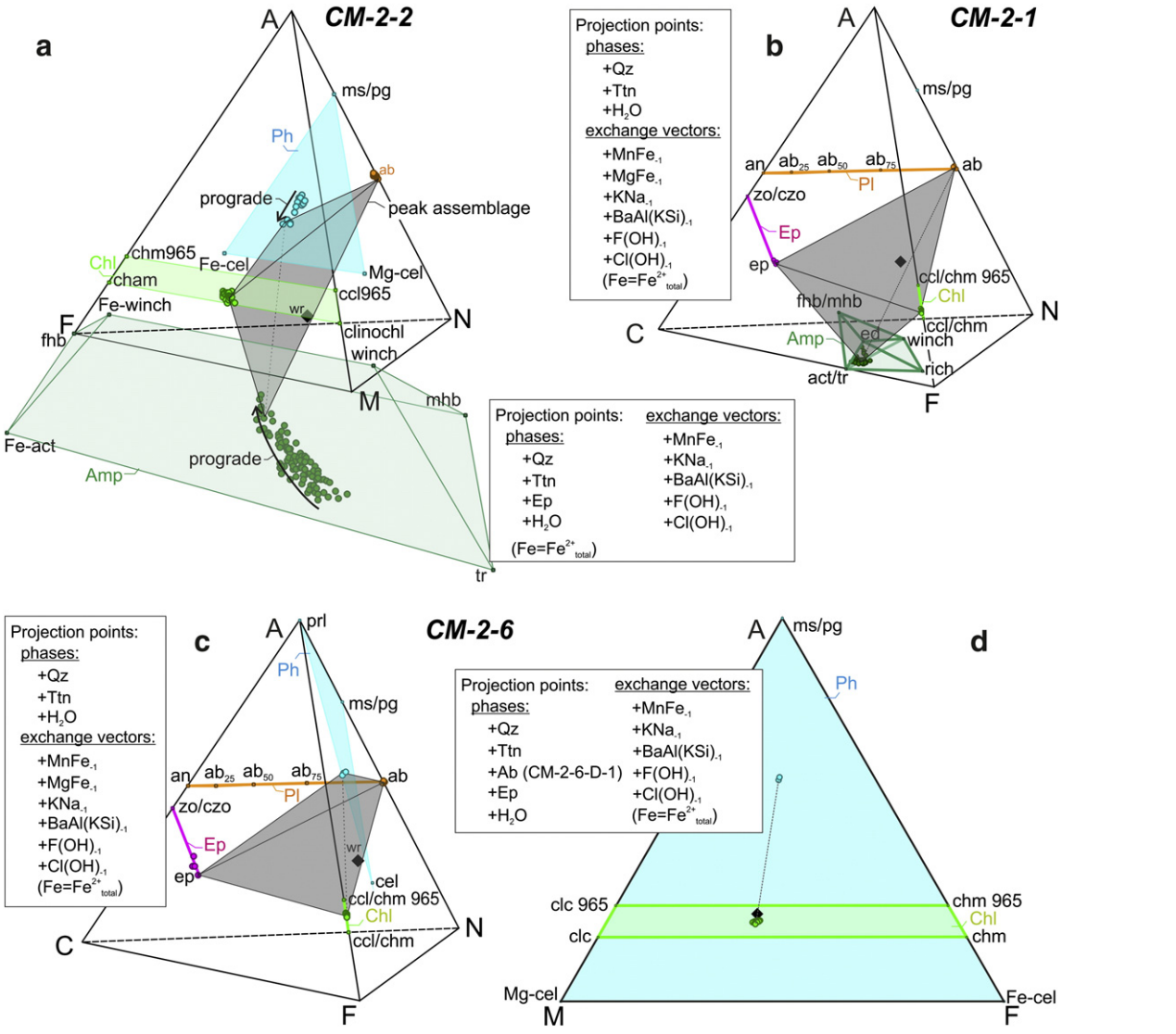

Fig. 12. Phase relationships for Group O1 metabasites from the Ozama shear zone in the AFMN (a; sample CM-2-2) and ACFN (b; sample CM-2-1) "deluxe" diagrams, and for sample CM-2-6 (Group A1-metabasite of the El Altar zone) in the ACFN (c) and AFM (d) diagrams. The minerals and bulk rock (wr) compositions are projected from the phases and exchange vectors indicated in each diagram. Chlorite end-members chm 965 and clc 965 refer to chamosite and clinochlore with atomic abundances of Fe-Mg, Al and Si of 9, 6 and 5 (per 10 O and 8 OH), respectively (Spear, 1993).

glaucophane would first grow in metabasite rocks with low Mg#, and the assemblage Gl + Chl + Ca/Na-Ca Amph would develop in Mg#-richer compositions upon increasing temperature and pressure (Figs. 11–34 in Spear, 1993; Fig. 5b herein). Hence, at the peak conditions calculated for our rocks, only metabasites abnormally enriched in FeO relative to MgO would be expected to form Fe-glaucophane. In Group O1 metabasites, MgO is steadily enriched relative to FeO (i.e., Mg# > 50) and in the AFM diagram of Fig. 5b their bulk composition plot out of the stability field of glaucophane. Accordingly, metabasites from the Ozama shear zone are hereinafter to be considered greenschists *s.s.* that underwent peak metamorphism in the limit greenschist/blueschists facies conditions.

8.2. Tectonic interpretation

Deformation and structural relations of the Maimón and Los Ranchos Formations were studied by Draper et al. (1996) and Draper and Gutiérrez-Alonso (1997) who assessed a top-to-the-north thrust sense of shear in the Ozama zone. These authors invoked the northward obduction of the adjacent Loma Caribe peridotite during the late Albian over the Maimón Formation and the structurally underlying Los Ranchos Formation as the ultimate cause for the major thrust deformation event. According to these authors, obduction and related transfer of heat from the hot peridotite slice to the underlying Ozama shear zone caused the inverted metamorphic-deformation gradient observed from the Ozama shear zone through the El Altar zone of the Maimón Formation to the Los Ranchos Formation, i.e., towards the N-NNE. The low-P (3 kbar) peak conditions and high thermal gradient (45 °C/km) proposed by Escuder-Viruete et al. (2002); Fig. 14 herein) would apparently agree with the peridotite obduction scenario. However, 3 kbar peak pressure translates into ~9 km depth below peridotite (assuming a mean density of 3.3 g/cm^3), which largely exceeds the thickness of the Loma Caribe peridotite tectonic slice (of barely 4 km maximum thickness in the Bonao-Maimón area; see Fig. 2 in Escuder-Viruete et al., 2010). Also, in the lack of a detailed thermal modeling, such a steep geothermal gradient is considered too high for a conductive scenario at shallow depths involving a thick volcanic-arc sequence.

With the data obtained in this study, the calculated pressure of ~8.2 kbar (i.e., 25.36 km − 3.3 g/cm^3-, or 28.85 km - in perhaps more realistic scenario of 2.9 g/cm^3 average density in order to account for overriding arc crust plus mantle) at ~380 °C in Ozama shear zone metabasites corresponds to a thermal gradients in the range of

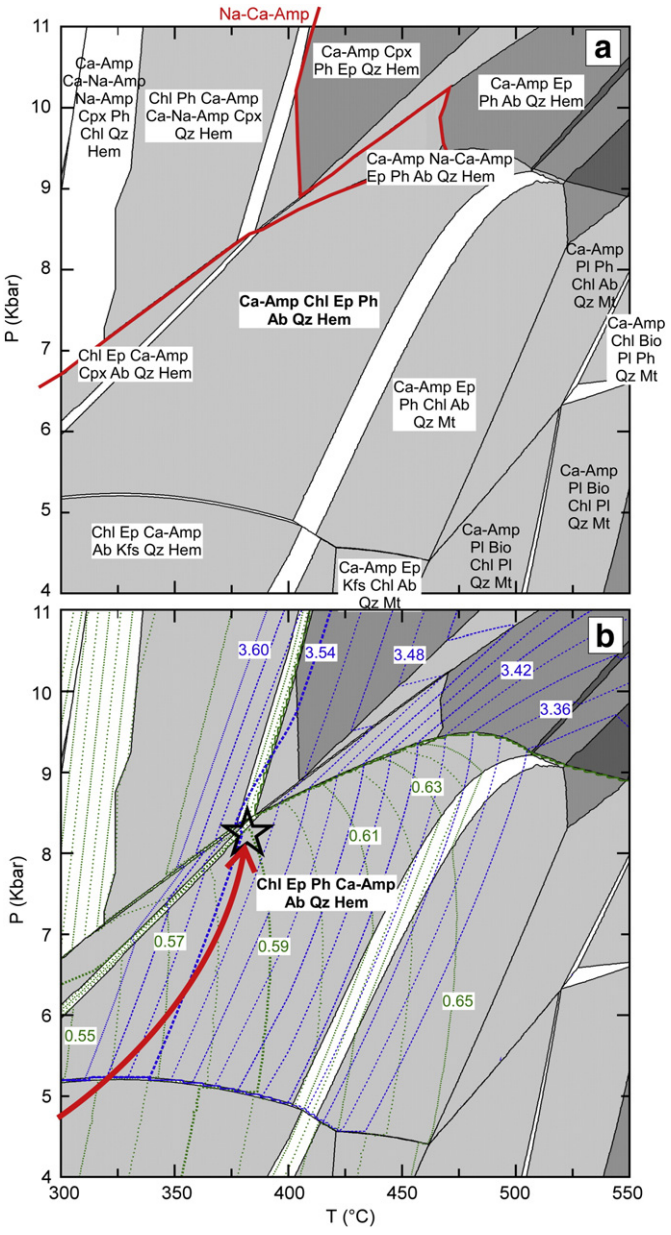

Fig. 13. (a) Isochemical P–T equilibrium phase diagram for sample CM-2-2 (Ozama shear zone) calculated with Perple_X [SiO_2 = 60.15, Al_2O_3 = 6.60, FeO = 8.05, MgO = 13.82, CaO = 6.47, Na_2O = 4.27, K_2O = 0.63, O_2 = 0.40 (percent molar units)]; the red line in the upper diagram indicates the presence of sodium-calcium amphibole in the assemblages at high pressure. Mineral abbreviations after Whitney and Evans (2010), except for amphibole composition denoted by the Na- Ca- or Na-Ca classification. The color code indicates thermodynamic variance from 3-variant (white) to 8-variant (dark gray). (b) Isopleths for Si (a.p.f.u.) in phengite (blue dashed lines) and Mg# in the chlorite (green dotted lines) are represented. In (b), the star indicates the peak metamorphic P–T conditions, and the red arrow (path) represents a warm geothermal gradient downdip along the top of the descending slab (see Fig. 14).

15.99 °C/km (3.3 g/cm^3) to 13.17 °C/km (2.9 g/cm^3), in any case much lower than inferred by Escuder-Viruete et al. (2002) (Fig. 14). According to these data, the relative high pressures and corresponding relatively cold thermal gradient undergone by rocks of the Maimón Formation cannot be easily conceptualized within the framework of overthrusting of a shallow hot peridotite slice over the volcanic-arc formation, as proposed by Draper and Gutiérrez-Alonso (1997), Draper et al. (1996) and Escuder-Viruete et al. (2002). The inferred depth of 25–29 km during metamorphism cannot be accounted for by the thickness of the Loma Caribe peridotite sheet. Instead, such thermal gradient and metamorphic depth is consistent with subduction of warm lithosphere (Peacock and Wang, 1999; Fig. 14), as expected for a young oceanic island-arc environment developed in the Early Cretaceous (c. 125–110 Ma for the Los Ranchos Formation: Cumming and Kesler, 1987; Cumming et al., 1982; Escuder-Viruete et al., 2006, 2007c; Kesler et al., 1991b, 2005; Kirk et al., 2014; Nelson et al., 2015; Torró et al., accepted; slightly older age inferred for the Maimón Formation: Horan, 1995; Torró et al., 2016, in press). The aforementioned gradient is also consistent with the conditions of other Cretaceous volcanic arc formations subducted during the Cretaceous-Early Tertiary in the Caribbean realm, such as the Villa del Cura complex, Venezuela (Smith et al., 1999), the Purial complex, Cuba (Garcia-Casco et al., 2008b and references therein), and the Blue Mountains, Jamaica (West et al., 2014 and references therein) (Fig. 14), and with the thermal conditions during syn-subduction exhumation of eclogite and blueschist facies rocks, as for example those of the Northern Dominican Republic Río San Juan complex (Escuder-Viruete and Pérez-Estaún, 2013; Escuder-Viruete et al., 2013a, 2013b; Krebs et al., 2008, 2011) (Fig. 14). Recently, Willner et al. (2016) have studied blueschist and greenschist rocks from Mt. Hibernia, Jamaica, both formed in a subduction-related accretionary complex. The peak conditions calculated by these authors for the greenschists rocks are very similar to those calculated here for the Ozama zone of the Maimón Formation (Fig. 14), further reinforcing our interpretation of subduction-related metamorphism in the Maimón Formation.

Subduction of both active and quiescent oceanic arcs into the mantle is broadly described, for instance, in the western part of the Philippine Sea plate, where immature small arcs smoothly subduct beneath the Eurasian plate (Ichikawa et al., 2016, and references therein). As it has been argumented, we discard the Ozama shear zone of the Maimón Formation being a metamorphic sole associated with peridotite obduction since 1) the thickness of the Ozama shear zone (~ 3.5 km) amply exceeds the average thicknesses (<500 m) of described soles and 2) its thermal gradient (~ 13–16 °C/km) is markedly lower than the 26–30 °C/km that characterizes soles (e.g., Wakabayashi and Dilek, 2000).

8.3. Constraints on tectonic models

All our attempts to date the metamorphic event that affected the Maimón rocks by using radiogenic isotopic techniques have been futile because of the very fine grained nature of metamorphic sheet silicates and the extremely low K_2O contents of amphibole. In order to constrain the timing of the metamorphism and deformation, we will follow the structural and stratigraphic framework of Draper and Gutiérrez-Alonso (1997), Draper et al. (1996) and Lewis et al. (2002). According to these workers, metamorphism and shear deformation in the Maimón and, to a lesser extent, the Los Ranchos formations developed previous to the deposition of the Albian Hatillo limestone, which unconformably overlies the Los Ranchos Formation and is not penetratively deformed. Invertebrate fauna at the base of the Hatillo Formation was dated as late Lower Albian by Myczynski and Iturralde-Vinent (2005). Hence, the Maimón Formation subducted and exhumed previous to c. 110 Ma. An onset of the subduction of the Proto-Caribbean at c. 135 Ma (Pindell et al., 2012), or even c. 126 Ma for the Hispaniola arc segment (Escuder-Viruete et al., 2014), would result in a minimum time lapse of 10–15 m.y. (e.g., from 126 to 110 Ma) which satisfactorily allows metamorphism in the greenschist and blueschist facies conditions to be developed (e.g., Maresch and Gerya, 2005) and the subsequent exhumation of the HP/LT metamorphic complexes (e.g., Baldwin et al., 2008).

Subduction of the Maimón Formation in the Early Cretaceous is coeval with subduction of MOR- and island arc-related units of the Río San Juan metamorphic complex (Escuder-Viruete and Pérez-Estaún,

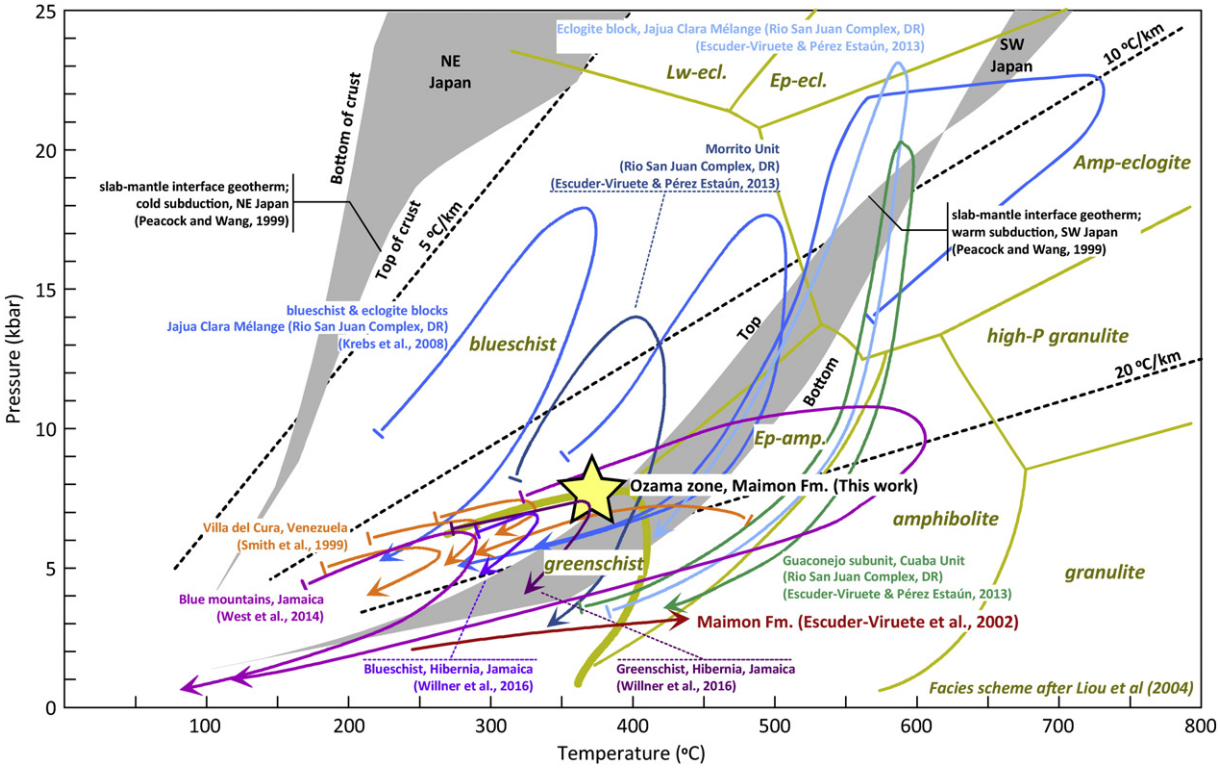

Fig. 14. Composite P–T diagram showing the calculated conditions of the Ozama shear zone of the Maimón Formation and other rock bodies in the region. The metamorphic conditions for the Ozama zone (star) locate in the greenschist to blueschist facies transition. Arrows represent the metamorphic P–T paths from high-pressure metamorphic complexes from Hispaniola (Maimón Formation after Escuder-Viruete et al., 2002; Río San Juan mélange after Krebs et al., 2008; Morrito unit, Jagua Clara serpentinite-matrix mélange, and Guaconejo subunit, after Escuder-Viruete and Pérez-Estaún, 2013a) and of subducted metamorphic volcanic arc sequences of the Caribbean (Blue Mountains after West et al., 2014; Mt. Hibernia after Willner et al., 2016; Villa del Cura after Smith et al., 1999). Slab-mantle interface geotherms (top and bottom of subducted oceanic crust) for cold and warm subduction are after Peacock and Wang (1999). The facies scheme is after Liou et al. (2004).

2013; Escuder-Viruete and Castillo-Carrión, 2016; Escuder-Viruete et al., 2013a, 2013b; Krebs et al., 2008, 2011). In this complex, arc-related units with coherent internal structure and high-pressure metamorphism include El Guineal (metarhyolite) and Puerca Gorda (metabasite) schists of the Morrito nappe and the Guaconejo subunit of the Cuaba unit; mega-blocks of metamorphosed rocks of basaltic protolith with arc-related signatures embedded in mélanges includes the Hicotea schists (see Table 1 in Escuder-Viruete et al., 2013a for the precise references on each unit). Rocks of the Morrito nappe reached blueschist and upper greenschist facies, similar to the studied rocks from the Ozama shear zone, while Guaconejo subunit rocks reached high-P garnet epidote amphibolite to eclogite facies. Geochemically, the protoliths of these units are classified as boninites, low-Ti IAT (variably depleted in LREE) and IAT, and hence they are broadly comparable to the geochemical affinities of the Maimón mafic volcanic rocks (Torró et al., 2016, in press). Escuder-Viruete et al. (2013a, 2013b) pointed out the manifest similarity of the mafic protoliths of the Morrito nappe and the Hicotea schists with the Early Cretaceous Caribbean volcanic rocks. Escuder-Viruete et al. (2013b) proposed that the arc protoliths of the la Cuaba unit began to subduct at c. 120–115 Ma, underwent prograde metamorphism at c. 110–95 Ma, reached peak conditions at 90–89 Ma and exhumed between 89 and 83 Ma following a clockwise P–T path (Fig. 14). Therefore, although arc-like rocks in the Río San Juan complex would have begun to subduct coeval to the Maimón Formation, their exhumation postdated that of the Maimón Formation. In Albian time (110–100 Ma), the rocks of the Río Verde complex in Cordillera Central of the Dominican Republic underwent metamorphism to the amphibolite facies shortly after formation in an Aptian-Albian rifted arc or back-arc basin setting (Escuder-Viruete et al., 2010) coeval with the Los Ranchos Formation magmatic front (Escuder-Viruete et al., 2006). Accordingly, Early Cretaceous metamorphism of arc-related volcanic units in the Hispaniola segment of the Caribbean island arc was not restricted to the Maimón Formation but represented a large-scale, regional event that affected the whole island arc section.

Upon these three following premises: 1) generation of the Maimón Formation in a forearc setting at c. 126 Ma (Lewis et al., 2000, 2002; Torró et al., 2016, in press); 2) metamorphism and deformation at 120–110 Ma linked to a subduction scenario (this work) and subsequent exhumation in the Early Cretaceous, shortly before c. 110 Ma (Draper and Gutiérrez-Alonso, 1997; Draper et al., 1996; Lewis et al., 2002); and 3) a regional-scale metamorphic event operating in the Hispaniola segment of the Caribbean arc, we envisage three possible scenarios. These scenarios correspond to tectonic models widely found in the literature for the subduction geometry of the western Proto-Caribbean margin during the Early Cretaceous: 1) subduction polarity reversal from E-dipping subduction of Farallon to W-dipping subduction of the Proto-Caribbean as a result of the collision of the Caribbean-Colombian Oceanic Plateau (CCOP) with the Greater Antilles arc (Kerr et al., 1999, 2003; Lidiak and Anderson, 2015), 2) initial (c. 135 Ma) W-dipping subduction of the Proto-Caribbean after the inception of a sinistral 'inter-American transform' that would have connected the E-dipping subduction zones fringing the western margins of North and South America (cf. Pindell et al., 2012) and 3) total consumption of the oceanic Mezcalera plate with two opposite dipping subduction zones below the Pacific Farallon plate and the Proto-Caribbean realm (Dickinson and Lawton, 2001; Escuder-Viruete et al., 2013a; Mann, 2007; Mann et al., 2007).

The polarity reversal hypothesis was embraced by Draper and Gutiérrez-Alonso (1997), Draper et al. (1996) and Lewis et al. (2002)

to explain the tectonic event causing the obduction of the Loma Caribe peridotite over the volcanic arc units (i.e., Maimón and Los Ranchos formations). In this framework, a coherent slice of the Early Cretaceous forearc could be dragged down in a new subduction zone developed after the collision of a Pacific plateau (Duarte Formation?) with the Pacific trench of the early Caribbean arc. Trench-plateau collision, and the ensuing break-off of the Pacific slab, would have allowed the flip of subduction, whose inception took place in the convergence front. Subduction of the new forearc at this early stage would have formed the Ozama zone of the Maimón Formation in the high-pressure greenschist/blueschist facies at shallow mantle depths, while only very shallow subduction, or crustal imbrications, affected the lower-grade and less intensely deformed the El Altar zone. The coeval arc-proximal Los Ranchos Formation did not subduct, but was affected by the associated tectonic event causing shallow, mostly brittle deformation. In this model, heating from an emplacing peridotite sheet is not needed. However, the model basically conforms to and re-interprets the structural relations described by Draper et al. (1996) and Draper and Gutiérrez-Alonso (1997) in the light of the new metamorphic data. According to these authors, once the west directed subduction/plateau collision took place, convergence between the Pacific and Proto-Caribbean lithospheres shifted towards the E-NE, i.e., towards the former back-arc, causing a subduction polarity reversal where a new more stable east directed subduction zone was established and steadily consumed Proto-Caribbean (i.e., Atlantic) lithosphere during the Late Cretaceous.

A major weakness against this scenario is indeed the timing of the polarity reversal. The polarity reversal event postulated by some authors to occur below the Greater Antilles island arc is placed in the Late Cretaceous (Lidiak and Anderson, 2015, and references therein); to fulfill the premises above described (and assumed by Draper et al., 1996), an unlikely different, c. 40 m.y. older reversal event should be invoked. The Duarte complex in Cordillera Central hosts the oldest CCOP rocks dated in the Greater Antilles (Lidiak and Anderson, 2015); Escuder-Viruete et al. (2007d) determined that the protoliths of the Duarte complex are most probably Albian (>96 Ma), i.e., they might have extruded at the time here bracketed for metamorphism of the Maimón Formation. It is hence suspect dating trench-Duarte complex collision and ensuing flip of subduction at ca. 120–110 Ma. Indeed, most recent kinematic reconstructions coincide to place the Early Cretaceous oceanic plateau in the eastern Pacific, southwestward away from the subduction zone during the Early and most of the Late Cretaceous (e.g., Kerr et al., 1999; Pindell et al., 2012; Fig. 40 in Lidiak and Anderson, 2015). Accordingly, a collision event including the choking of a buoyant oceanic plateau and ensuing flipping of subduction in the Early Cretaceous is difficult to conceive.

In the second scenario, adapted from the model of Pindell et al. (2012), Early Cretaceous (c. 135 Ma) onset of WSW-directed subduction of the Proto-Caribbean lithosphere occurred in the context of a trench-to-trench transform fault connecting the W-facing subduction zones in the western flank of the Americas (Fig. 15a). Relative motion along the trench-trench transform zone was mainly transpressive and the strong sinistral shear component was accommodated by a series of duplex bounded by anticlockwise transform faults that segmented both the pre 135 Ma volcanic arc and the newly born (i.e., post 135 Ma) Caribbean arc crust. Convergence and subduction of the Proto-Caribbean at an oblique angle to the trench, likely aided by the interaction with buoyant features such as the Proto-Caribbean ridge, could have forced part of the Caribbean arc crust to subduct along one of these intra-arc faults. This setting for an intra-Caribbean arc trench (Fig. 15b–c) would favor subduction of a forearc portion (i.e., the Maimón Formation), while other volcanic arc domains (i.e., the arc axis, represented by the Los Ranchos Formation: Escuder-Viruete et al., 2006; Torró et al., accepted) would have escaped subduction. Our model can be envisaged as a sort of subduction erosion setting, allowing other elements of the upper plate, such as those present in

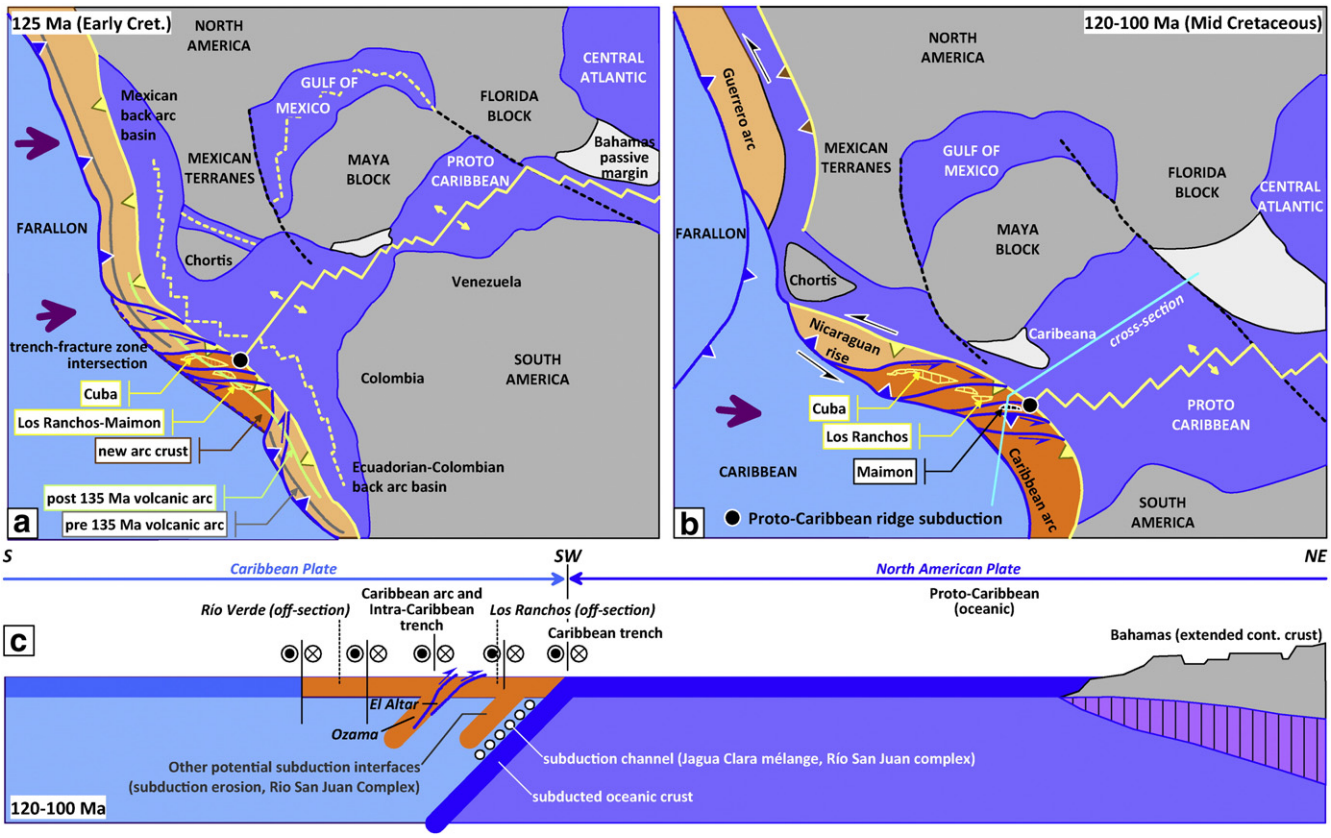

Fig. 15. Possible tectonic scenario for the development of high-pressure in the Maimón Formation, following Pindell and Kennan (2009) and Pindell et al. (2012). See text for details.

the Río San Juan complex, to be incorporated into subduction (Fig. 15). It hence adequately explains a regional-scale, major tectonic event resulting in deformation and metamorphism operating synchronously along major portions of the Hispaniola island arc segment and accounts for an intense decrease in arc magmatism and the deposition of the thick reefal carbonate sequence of the Hatillo Formation (cf. Bowin, 1966; Escuder-Viruete et al., 2006; Kesler et al., 2005).

Finally, the arc–arc collision model proposed by Escuder-Viruete et al. (2013a); Fig. 12 therein), in which two converging arcs with opposite dipping subduction zones collided at c. 120 Ma after consumption of the intervening oceanic Mezcalera plate (Dickinson and Lawton, 2001; Mann, 2007), would also account for the regional scale subduction-collision metamorphic event registered in Early Cretaceous arc-related units of Hispaniola. This model, however, predicts volcanic arc development as old as Jurassic and generalized arc–arc collision in the Caribbean realm with progressive shift of the collision zone from N to S (Early Cretaceous coordinates). The lack of Jurassic volcanic arc sections in Cuba, Hispaniola and Puerto Rico and of Early Cretaceous subduction/collision-related metamorphic complexes involving volcanic arc sections in Cuba and Puerto Rico (to the North and South of Hispaniola, respectively) (Lidiak and Anderson, 2015) make this model weak. To be noted is that the volcanic-arc related El Purial (eastern Cuba) and Mabujina (central Cuba) complexes, that subducted/collided at 75–70 Ma (Garcia-Casco et al., 2008a and references therein) and c. 90 Ma (Rojas-Agramonte et al., 2011), respectively, cannot be related to the Early Cretaceous event discussed here. We hence prefer a more local model such as the one presented in Fig. 15.

9. Conclusions

P–T calculations based on detailed examination of mineral assemblages and mineral chemistry of selected metabasites from the Ozama shear zone of the Maimón Formation whose protoliths are only weakly altered and approximate the composition of pristine arc basalts have allowed the determination of higher peak pressure conditions than previously estimated. Our estimate of ~8.2 kbar at 380 °C is consistent with metamorphism in the greenschist-blueschist facies transition, burial depths of 25–29 km and thermal gradient in the range 13–16 °C/km. We suggest that metamorphism was triggered by subduction of a forearc segment (i.e., the Maimón Formation) in the late Early Cretaceous times in the framework of a major tectonic event that affected the Hispaniola island arc segment.

Acknowledgements

This research has been funded by Spanish project CGL2012-36263, Catalan project 2014-SGR-1661 and a FPU Ph.D. grant to L.T. by the Ministerio de Educación of the Spanish Government, and received support for analyses at CIC from the University of Granada. L. Butjosa and T.H. Aiglsperger participated in the field works in the Dominican Republic. The help and hospitality extended by the staff at Cerro de Maimón mine are also gratefully acknowledged, as well as the technical support in EMP sessions by Dr. X. Llovet. We are grateful to Dr. J. Escuder-Viruete and Dr. W.V. Maresch for sound reviews and to Dr. M. Scambelluri for the competent editorial handling.

References

Agard, P., Yamato, P., Jolivet, L., Burov, E., 2009. Exhumation of oceanic blueschists and eclogites in subduction zones: timing and mechanisms. Earth-Science Reviews 92, 53–79.

Baldwin, S.L., Webb, L.E., Monteleone, B.D., 2008. Late Miocene coesite-eclogite exhumed in the Woodlark Rift. Geology 36, 735–738.

Blacic, J.D., 1975. Plastic deformation mechanism in quartz: the effect of water. Tectonophysics 27, 271–294.

Blanco-Quintero, I.F., Garcia-Casco, A., Rojas-Agramonte, Y., Rodríguez Vega, A., Lázaro, C., Iturralde-Vinent, M.A., 2010. Metamorphic evolution of subducted hot oceanic crust, La Corea mélange, Cuba. American Journal of Science 310, 889–915.

Blanco-Quintero, I.F., Rojas-Agramonte, Y., Garcia-Casco, A., Kröner, A., Mertz, D.F., Lázaro, C., Blanco-Moreno, J., Renne, P.R., 2011. Timing of subduction and exhumation in subduction channel: evidence from slab melts from La Corea Mélange (eastern Cuba). Lithos 127, 86–100.

Boiteau, A., Michard, A., Saliot, P., 1972. Métamporphisme de haute pression dans le complexe ophiolitique du Purial (Oriente,Cuba). Comptes Rendus de l'Académie des Sciences Paris 274 (série D), 2137–2140.

Boschman, L.M., van Hinsbergen, D.J.J., Torsvik, T.H., Spakman, W., Pindell, J.L., 2014. Kinematic reconstruction of the Caribbean region since the Early Jurassic. Earth-Science Reviews 138, 102–136.

Bowin, C.O., 1960. Geology of Central Dominican Republic. (Ph.D. thesis). Princeton Univ., Princeton, N.J (211 pp.).

Bowin, C.O., 1966. Geology of the central Dominican Republic. Geological Society of America Memoirs 98, 11–84.

Carreras, J., Druguet, E., Griera, A., 2005. Shear zone-related folds. Journal of Structural Geology 27, 1229–1251.

Coggon, R., Holland, T.J.B., 2002. Mixing properties of phengitic micas and revised garnet-phengite thermobarometers. Journal of Metamorphic Geology 20, 683–696.

Connolly, J.A.D., 1990. Multivariable phase-diagrams - an algorithm based on generalized thermodynamics. American Journal of Science 290, 666–718.

Connolly, J.A.D., 2005. Computation of phase equilibria by linear programming: a tool for geodynamic modeling and its application to subduction zone decarbonation. Earth and Planetary Science Letters 236, 524–541.

Cumming, G.L., Kesler, S.E., 1987. Lead isotopic composition of the oldest volcanic rocks of the Eastern Greater Antilles island arc. Chemical Geology 65, 15–23.

Cumming, G.L., Kesler, S.E., Krstic, D., 1982. Source of lead in sulfide ore at the Pueblo Viejo gold-silver oxide deposit, Dominican Republic. Economic Geology 77, 1939–1941.

Dale, J., Powell, R., White, R.W., Elmer, F.L., Holland, T.J.B., 2005. A thermodynamic model for Ca-Na clinoamphiboles in Na_2O-CaO-FeO-MgO-Al_2O_3-SiO_2-H_2O-O for petrological calculations. Journal of Metamorphic Geology 23, 771–791.

Dickinson, W., Lawton, T., 2001. Carboniferous to Cretaceous assembly and fragmentation of Mexico. Geological Society of America Bulletin 113, 1142–1160.

Donnelly, T.W., Beets, D., Carr, M.J., Jackson, T., Klaver, G., Lewis, J., Maury, R., Schellenkens, H., Smith, A.L., Wadge, G., Westercamp, D., 1990. History and tectonic setting of Caribbean magmatism. In: Dengo, G., Case, J.E. (Eds.), The Caribbean Region. Geological Society of America, The Geology of North America, H, Boulder, Colorado, pp. 339–374.

Draper, G., Gutiérrez-Alonso, G., 1997. La estructura del cinturón de Maimón en la Isla de Hispaniola y sus implicaciones geodinámicas. Revista de la Sociedad Geológica de España 10, 281–299.

Draper, G., Lewis, J.F., 1991. Metamorphic belts in Central Hispaniola. In: Mann, P., Draper, G., Lewis, J.F. (Eds.), Geologic and Tectonic Development of the North America-Caribbean Plate Boundary in Hispaniola. Geological Society of America Special Papers Vol. 262, pp. 173–185.

Draper, G., Gutiérrez, G., Lewis, J.F., 1996. Thrust emplacement of the Hispaniola peridotite belt: orogenic expression of the mid Cretaceous Caribbean arc polarity reversal? Geology 24, 1143–1146.

Escuder-Viruete, J., Castillo-Carrión, M., 2016. Subduction of fore-arc crust beneath an intra-oceanic arc: the high-P Cuaba mafic gneisess and amphibolites of the Rio San Juan Complex, Dominican Republic. Lithos 262, 298–319.

Escuder-Viruete, J., Pérez-Estaún, A., 2013. Contrasting exhumation P–T paths followed by high-P rocks in the northern Caribbean subduction-accretionary complex: insights from the structural geology, microtextures and equilibrium assemblage diagrams. Lithos 160, 117–144.

Escuder-Viruete, J., Hernaiz-Huerta, P.P., Draper, G., Gutiérrez, G., Lewis, J.F., Pérez-Estaún, A., 2002. Metamorfismo y estructura de la Formación Maimón y los Complejos Duarte y Río Verde, Cordillera Central Dominicana: implicaciones en la estructura y evolución del primitivo Arco-Isla Caribeño. Acta Geologica Hispanica 37, 123–162.

Escuder-Viruete, J., Díaz de Neira, A., Hernáiz Huerta, P.P., Monthel, J., García Senz, J., Joubert, M., Lopera, E., Ullrich, T., Friedman, R., Mortensen, J., Pérez-Estaún, A., 2006. Magmatic relationships and ages of Caribbean island-arc tholeiites, boninites and related felsic rocks, Dominican Republic. Lithos 90, 161–186.

Escuder-Viruete, J., Contreras, F., Stein, G., Urien, P., Joubert, M., Pérez-Estaún, A., Friedman, R., Ullrich, T., 2007a. Magmatic relationships between adakites, magnesian andesites and Nb-enriched basalt-andesites from Hispaniola: record of a major change in the Caribbean island arc magma sources. Lithos 99, 151–177.

Escuder-Viruete, J., Contreras, F., Joubert, M., Urien, P., Stein, G., Weis, D., Pérez-Estaún, A., 2007b. Tectónica y geoquímica de la Formación Amina: registro del arco isla Caribeño primitivo en la Cordillera Central, República Dominicana. Boletín Geológico y Minero 118, 221–242.

Escuder-Viruete, J., Diaz de Neira, A., Hernaiz-Huerta, P.P., Garcia-Senz, J., Monthel, J., Joubert, M., Lopera, E., Ulrich, T., Friedan, R., Weis, D., Pérez-Estaún, A., 2007c. Implicaciones tectonomagmáticas y edad de las toleítas de arco-isla, boninitas y rocas ácidas relacionadas de la formación Los Ranchos, Cordillera Oriental, Republica Dominicana. Boletín Geológico y Minero 118, 195–220.

Escuder-Viruete, J., Pérez-Estaún, A., Contreras, F., Joubert, M., Weis, D., Ullrich, T.D., Spadea, P., 2007d. Plume mantle source heterogeneity through time: insights from the Duarte Complex, Hispaniola, northeastern Caribbean. Journal of Geophysical Research 112, B04203.

Escuder-Viruete, J., Joubert, M., Urien, P., Friedman, R., Weis, D., Ullrich, T., Pérez-Estaún, A., 2008. Caribbean island-arc rifting and back-arc basin development in the Late Cretaceous: geochemical, isotopic and geochronological evidence from Central Hispaniola. Lithos 104, 378–404.

Escuder-Viruete, J., Pérez-Estaún, A., Weis, D., Friedman, R., 2010. Geochemical characteristics of the Río Verde Complex, Central Hispaniola: implications for the paleotectonic reconstruction of the Lower Cretaceous Caribbean island-arc. Lithos 114, 168–185.

Escuder-Viruete, J., Pérez-Estaún, A., Booth-Rea, G., Valverde-Vaquero, P., 2011. Tectonomorphic evolution of the Samaná complex, northern Hipaniola: implications for the burial and exhumation of high-pressure rocks in a collisional accretionary wedge. Lithos 125, 190–210.

Escuder-Viruete, J., Valverde-Vaquero, P., Rojas-Agramonte, Y., Gabites, J., Pérez-Estaún, A., 2013a. From intra-oceanic subduction to arc accretion and arc–continent collision: insights from the structural evolution of the Río San Juan metamorphic complex, northern Hispaniola. Journal of Structural Geology 46, 34–56.

Escuder-Viruete, J., Valverde-Vaquero, P., Rojas-Agramonte, Y., Gabites, J., Castillo-Carrión, M., Pérez-Estaún, A., 2013b. Timing of deformational events in Río San Juan complex: implications for the tectonic controls on the exhumation of high-P rocks in the northern Caribbean subduction-accretionary prism. Lithos 177, 416–435.

Escuder-Viruete, J., Castillo-Carrión, M., Pérez-Estaún, A., 2014. Magmatic relationships between depleted mantle harzburgites, boninitic cumulate gabbros and subduction-related tholeiitic basalts in the Puerto Plata ophiolitic complex, Dominican Republic: implication for the birth of the Caribbean island-arc. Lithos 196-197, 261–280.

Fisher, G.W., 1989. Matrix analysis of metamorphic mineral assemblages and reactions. Contributions to Mineralogy and Petrology 102, 69–77.

Fisher, G.W., 1993. An improved method for algebraic analysis of metamorphic mineral assemblages. American Mineralogist 78, 1257–1261.

Franz, G., Liebscher, A., 2004. Physical and chemical properties of the epidote minerals: an introduction. In: Franz, G., Liebscher, A. (Eds.), Reviews in Mineralogy and Geochemistry: Epidote vol. 56. Mineralogical Society of America and Geochemical Society, Washington, pp. 1–82.

Fuhrman, M.L., Lindsley, D.H., 1988. Ternary-feldspar modeling and thermometry. American Mineralogist 73, 201–215.

Galley, A.G., Hannington, M.D., Jonasson, I.R., 2007. Volcanogenic massive sulphide deposits. In: Goodfellow, W.D. (Ed.), Mineral Deposits of Canada: A Synthesis of Major Deposit-Types, District Metallogeny, the Evolution of Geological Provinces, and Exploration Methods. Geological Association of Canada, Mineral Deposits Division, Special Publication Vol. 5, pp. 141–161.

Garcia-Casco, A., 2007. Magmatic paragonite in trondhjemites from the Sierra del Convento mélange, Cuba. American Mineralogist 92, 1232–1237.

Garcia-Casco, A., Sanchez-Navas, A., Torres-Roldan, R.L., 1993. Disequilibrium decomposition and breakdown of muscovite in high P–T gneisses, Betic Alpine Belt (southern Spain). American Mineralogist 78, 158–177.

Garcia-Casco, A., Torres Roldán, R.L., Millán Trujillo, G., Monié, P., Schneider, J., 2002. Oscillatory zoning in eclogitic garnet and amphibole, northern serpentinite melange, Cuba: a record of tectonic instability during subduction? Journal of Metamorphic Geology 20, 581–598.

Garcia-Casco, A., Torrés-Roldán, R.L., Iturralde-Vinent, M.A., Millán, G., Núñez-Cambra, K., Lázaro, C., Rodríguez-Vega, A., 2006. High pressure metamorphism of ophiolites in Cuba. Geologica Acta 4, 63–88.

Garcia-Casco, A., Iturralde-Vinent, M.A., Pindell, J., 2008a. Latest Cretaceous collision/accretion between the Caribbean plate and Caribeana: origin of metamorphic terranes in the Greater Antilles. International Geology Review 50, 781–809.

Garcia-Casco, A., Lázaro, C., Rojas-Agramonte, Y., Kröner, A., Torres Roldán, R.L., Nuñez, K., Millán, G., Neubaurer, F., Quintero, I., 2008b. Partial melting and counterclockwise P–T path of subducted oceanic crust (Sierra del Convento, E Cuba). Journal of Petrology 49, 129–161.

Gerya, T.V., 2011. Chapter 2: intra-oceanic subduction zones. In: Brown, D., Ryan, P.D. (Eds.), Arc–Continent CollisionFrontiers in Earth Sciences. Springer-Verlag, Germany, pp. 23–51.

Gerya, T.V., Stoeckhert, B., Perchuk, A.L., 2002. Exhumation of high-pressure metamorphic rocks in a subduction channel. A numerical simulation. Tectonics 21, 1–19.

Gilgen, S.A., Diamond, L.W., Mercolli, I., 2016. Sub-seafloor epidosite alteration: timing, depth and stratigraphic distribution in the Semail ophiolite, Oman. Lithos 260, 191–210.

Green, E., Holland, T., Powell, R., 2007. An order–disorder model for omphacitic pyroxenes in the system jadeite-diopside-hedenbergite-acmite, with applications to eclogitic rocks. American Mineralogist 92, 1181–1189.

Guidotti, C.V., 1984. Micas in metamorphic rocks. Reviews in Mineralogy and Geochemistry 13, 357–455.

Hawkins, J.W., Bloomer, S.H., Evans, C.A., Melchior, J.T., 1984. Evolution of intra-oceanic arc-trench systems. Tectonophysics 102, 175–205.

Hawthorne, F.C., Oberti, R., Harlow, G.E., Maresch, W.V., Martin, R.F., Schumacher, J.C., Welch, M.D., 2012. IMA report: nomenclature of the amphibole supergroup. American Mineralogist 97, 2031–2048.

Holland, T.J.B., Powell, R., 1998. An internally consistent thermodynamic data set for phases of petrological interest. Journal of Metamorphic Geology 16, 309–343.

Holland, T., Baker, J., Powell, R., 1998. Mixing properties and activity-composition relationships of chlorites in the system MgO-FeO-Al_2O_3-SiO_2-H_2O. European Journal of Mineralogy 10, 395–406.

Horan, S.L., 1995. The Geochemistry and Tectonic Significance of the Maimón-Amina Schists, Cordillera Central, Dominican Republic. Unpublished M.S. thesis. University of Florida, Gainesville, p. 172 pp.

Ichikawa, H., Yamamoto, S., Kawai, K., Kameyama, M., 2016. Estimate of subduction rate of island arcs to the deep mantle. Journal of Geophysical Research: Solid Earth 121, 5447–5460.

Jicha, B.R., Jagoutz, O., 2015. Magma production rates for intraoceanic arcs. Elements 11, 105–112.

Jolly, W.T., Lidiak, E.G., Dickin, A.P., Wu, T.W., 2001. Secular geochemistry of central Puerto Rican Island arc lavas: constraints on Mesozoic tectonism in the Eastern Greater Antilles. Journal of Petrology 42, 2197–2214.

Kerr, A.C., Iturralde-Vinent, M.A., Saunders, A.D., Babbs, T.L., Tarney, J., 1999. New plate tectonic model of the Caribbean: implications from a geochemical reconnaissance of Cuban Mesozoic volcanic rocks. Geological Society of America Bulletin 111, 2–20.

Kerr, A.C., White, R.V., Thompson, P.M.E., Tarney, J., Saunders, A.D., 2003. No oceanic plateau-no Caribbean plate? The seminal role of an oceanic plateau in Caribbean plate evolution. The Circum Gulf of Mexico and Caribbean. In: Bartolini, C., Buffler, R.T., Blickwedge, J. (Eds.), Hydrocarbon Habitats Basin Formation and Plate Tectonics. American Association of Petroleum Geologists Memoirs Vol. 79, pp. 126–168.

Kesler, S., Russell, E.N., Reyes, C., Santos, L., Rodriguez, A., Fondeur, L., 1991a. Geology of the Maimon Formation, Dominican Republic. In: Mann, P., Draper, G., Lewis, J.F. (Eds.), Geologic and Tectonic Development of the North America-Caribbean Plate Boundary in Hispaniola. Geological Society of America Special Papers Vol. 262, pp. 173–185.

Kesler, S.E., Russell, N., Polanco, J., McCurdy, K., Cumming, G.L., 1991b. Geology and geochemistry of the early Cretaceous Los Ranchos Formation, central Dominican Republic. In: Mann, P., Draper, G., Lewis, J.F. (Eds.), Geologic and Tectonic Development of the North American: Caribbean Plate Boundary in Hispaniola. Geological Society of America Special Papers Vol. 262, pp. 187–201.

Kesler, S.E., Campbell, I.H., Allen, C.M., 2005. Age of the Los Ranchos Formation, Dominican Republic: timing and tectonic setting of primitive island arc volcanism in the Caribbean region. Geological Society of America Bulletin 117, 987–995.

Kirk, J.D., Ruiz, J., Kesler, S.E., Simon, A., Muntean, J.L., 2014. Re-Os age of the Pueblo Viejo epithermal deposit, Dominican Republic. Economic Geology 109, 503–512.

Krebs, M., Maresch, W.V., Schertl, H.-P., Münker, C., Baumann, A., Draper, G., Idleman, B., Trapp, E., 2008. The dynamics of intra-oceanic subduction zones: a direct comparison between fossil petrological evidence (Rio San Juan Complex, Dominican Republic) and numerical simulation. Lithos 103, 106–137.

Krebs, M., Schertl, H.P., Maresch, W.V., Draper, G., 2011. Mass flow in serpentinite-hosted subduction channels: P–T–t path patterns of metamorphic blocks in the Rio San Juan mélange (Dominican Republic). Journal of Asian Earth Sciences 42, 569–595.

Lázaro, C., Garcia-Casco, A., Rojas-Agramonte, Y., Kröner, A., Neubauer, F., Iturralde-Vinent, M., 2009. Fifty-five-million-year history of oceanic subduction and exhumation at the northern edge of the Caribbean plate (Sierra del Convento). Journal of Metamorphic Geology 27, 19–40.

Lebrón, M.C., Perfit, M.R., 1994. Petrochemistry and tectonic significance of Cretaceous island-arc-rocks, Cordillera Oriental, Dominican Republic. Tectonophysics 229, 69–100.

Lewis, J.F., Draper, G., 1990. Geology and tectonic evolution of the Northern Caribbean margin. In: Dengo, G., Case, J.E. (Eds.), The Caribbean Region. Geological Society of America, The Geology of North America, H, Boulder, Colorado, pp. 77–140.

Lewis, J.F., Astacio, V.A., Espaillat, J., Jiménez, J., 2000. The occurrence of volcanogenic massive sulfide deposits in the Maimón Formation, Dominican Republic: the Cerro de Maimón, Loma Pesada and Loma Barbuito deposits. In: Sherlock, R., Barsch, R., Logan, A. (Eds.), VMS Deposits of Latin America. Geological Society of Canada Special Publications Vol. 2, pp. 213–239.

Lewis, J.F., Escuder Viruete, J., Hernaiz Huerta, P.P., Gutiérrez, G., Draper, G., 2002. Subdivisión geoquímica del arco de isla Circum-Caribeño, Cordillera Central Dominicana: implicaciones para la formación, acreción y crecimiento cortical en un ambiente Intraoceánico. Acta Geologica Hispanica 37, 81–122.

Lewis, J.F., Draper, G., Proenza, J.A., Espaillat, J., Jiménez, J., 2006. Ophiolite-related ultramafic rocks (serpentinites) in the Caribbean region: a review of the occurrence, composition, origin, emplacement and Ni-laterite soil formation. Geologica Acta 4, 237–263.

Lidiak, E.G., Anderson, T.H., 2015. Evolution of the Caribbean plate and origin of the Gulf of Mexico in light of plate motions accommodated by strike-slip faulting. In: Anderson, T.H., Didenko, A.N., Johnson, C.L., Khanchuk, A.I., MacDonald Jr., J.H. (Eds.), Late Jurassic Margin of Laurasia—A Record of Faulting Accommodating Plate Rotation. Geological Society of America Special Papers Vol. 513 (SPE513–01).

Liou, J.G., Tsujimori, T., Zhang, R.Y., Katayama, I., Maruyama, S., 2004. Global UHP metamorphism and continental subduction/collision: the Himalayan model. International Geology Review 46, 1–27.

Lister, G.S., 1977. Discussion: crossed girdle c-axis fabrics in quartzites plastically deformed by plane strain and progressive simple shear. Tectonophysics 39, 51–54.

Mann, P., 2007. Overview of the tectonic history of northern Central America. The Geological Society of America Special Papers 428, 1–19.

Mann, P., Draper, G., Lewis, J.F., 1991. An overview of the geologic and tectonic development of Española. In: Mann, P., Draper, G., Lewis, J.F. (Eds.), Geologic and Tectonic Development of the North-America-Caribbean Plate Boundary in Española. Geological Society of America Special Papers Vol. 262, pp. 1–28.

Mann, P., Calais, E., Ruegg, J.C., DeMets, C., Jansma, P.E., Mattioli, G.S., 2002. Oblique collision in the northeastern Caribbean from GPS measurements and geological observations. Tectonics 21, 1057.

Mann, P., Rogers, R.D., Gahagan, L., 2007. Overview of plate tectonic history and its unresolved tectonic problems. In: Bundschuh, J., Alvarado, G. (Eds.), Central America: Geology, Resources and Hazards. Taylor y Francis, London, pp. 201–237.

Maresch, W.V., Gerya, T.V., 2005. Blueschists and blue amphiboles: how much subduction do they need? International Geology Review 47, 688–702.

Martín, M., Draper, G., 1999. Mapa geológico de la hoja 6172-I (Hatillo) a escala 1:50 000 (SYSMIN, Proyecto C). Consorcio ITGE-PROINTEC-INYPSA. Dirección General de Minería, Santo Domingo.

Massonne, H.J., Schreyer, W., 1987. Phengite geobarometry based on the limiting assemblage with K-feldspar, phlogopite, and quartz. Contributions to Mineralogy and Petrology 96, 212–224.

Massonne, H.J., Szpurka, Z., 1997. Thermodynamic properties of white micas on the basis of high-pressure experiments in the systems K_2O-MgO-Al_2O_3-SiO_2-H_2O and K_2O-FeO-Al_2O_3-SiO_2-H_2O. Lithos 41, 229–250.

Massonne, H.J., Willner, A.P., 2008. Phase relations and dehydration behaviour of psammopelite and mid-ocean ridge basalt at very low-grade to low-grade metamorphic conditions. European Journal of Mineralogy 20, 867–879.
Millán, G., 1996. Metamorfitas de la asociación ofiolítica de Cuba. In: Iturralde-Vinent, M.A. (Ed.), Ofiolitas y Arcos Volcánicos de Cuba. Miami, USA, IGCP Project 364 Special Contribution Vol. 1, pp. 131–146.
Myczynski, R., Iturralde-Vinent, M., 2005. The Late Lower Albian invertebrate fauna of the Rio Hatillo Formation of Pueblo Viejo, Dominican Republic. Caribbean Journal of Science 41, 782–796.
Nagle, F., 1974. Blueschist, eclogite, paired metamorphic belts, and the early tectonic history of Hispaniona. Geological Society of America Bulletin 84, 1461–1466.
Nelson, C.E., Stein, H.J., Dominguez, H., Carrasco, C., Barrie, T., Torró, L., Proenza, J., 2015. Re-Os dating of molybdenite from the Pueblo Viejo (Au-Ag-Cu-Zn) and Douvray Cu-Au districts. Economic Geology 110, 1101–1110.
Peacock, S.M., Wang, K., 1999. Seismic consequences of warm versus cool subduction zone metamorphism: examples from northeast and southwest Japan. Science 286, 937–939.
Pindell, J.L., Kennan, L., 2009. Tectonic evolution of the Gulf of Mexico, Caribbean and northern South America in the mantle reference frame: an update. In: James, K., Lorente, M.A., Pindell, J. (Eds.), The Geology and Evolution of the Region between North and South America. Geological Society of London Special Publication Vol. 328, pp. 1–55.
Pindell, J.L., Maresch, W.V., Martens, U., Stanek, K.P., 2012. The Greater Antillean Arc: Early Cretaceous origin and proposed relationship to Central American subduction mélanges: implications for models of Caribbean evolution. International Geology Review 54, 131–143.
Pouchou, J.L., Pichoir, F., 1985. "PAP" (phi-rho-z) procedure for improved quantitative microanalysis. In: Armstrong, J.T. (Ed.), Microbeam Analysis. San Francisco Press, San Francisco, pp. 104–106.
Reagan, M.K., Hanan, B.B., Heizler, M.T., Hartman, B.S., Hickey-Vargas, R., 2008. Petrogenesis of volcanic rocks from Saipan and Rota, Mariana Islands, and implications for the evolution of nascent island arc. Journal of Petrology 49, 441–464.
Reagan, M.K., Ishizuka, O., Tsukuaba, H., Stern, R.J., Kelley, K.A., Ohara, Y., Blichert-Toft, J., Bloomer, S.H., Cash, J., Fryer, P., Hanan, B.B., Hickey Vargas, R., Ishii, T., Kimura, J.I., Peate, D.W., Rowe, M.C., Woods, M., 2010. Forearc basalts and subduction initiation in the Izu-Bonin-Mariana system. Geochemistry, Geophysics, Geosystems 11. http://dx.doi.org/10.1029/2009GC002871.
Rojas-Agramonte, Y., Kröner, A., Garcia-Casco, A., Somin, M., Iturralde-Vinent, M.A., Mattinson, J.M., Millán Trujillo, G., Sukar, K., Pérez Rodríguez, M., Carrasquilla, S., Wingate, M.T.D., Liu, D.Y., 2011. Timing and evolution of Cretaceous island arc magmatism in Central Cuba: implications for the history of arc system in the Northwestern Caribbean. Journal of Geology 119, 619–640.
Schmid, S.M., Casey, M., 1986. Complete fabric analysis of some commonly observed quartz c-axis patterns. Mineral and rock deformation: laboratory studies-the Patterson volume. Geophysical Monograph 36, 263–286.
Schneider, J., Bosch, D., Monié, P., Guillot, S., Garcia-Casco, A., Lardeaux, J.M., Torres-Roldán, R.L., Millán-Trujillo, G., 2004. Origin and evolution of the Escambray Massif (Central Cuba): an example of HP/LT rocks exhumed during intraoceanic subduction. Journal of Metamorphic Geology 22, 227–247.
Shand, S.J., 1943. Eruptive Rocks. Their Genesis, Composition, Classification, and Their Relation to Ore-Deposits with a Chapter on Meteorite. John Wiley & Sons, New York (360 pp.).
Simpson, G.D.H., Thompson, A.B., Connolly, J.A.D., 2000. Phase relations, singularities and thermobarometry of metamorphic assemblages containing phengite, chlorite, biotite, K-feldspar, quartz and H_2O. Contributions to Mineralogy and Petrology 139, 555–569.
Smith, C.A., Sisson, V.B., Avé Lallemant, H.G., Copeland, P., 1999. Two contrasting pressure–temperature paths in the Villa de Cura blueschist belt, Venezuela: possible evidence for Late Cretaceous initiation of subduction in the Caribbean. Geological Society of America Bulletin 111, 831–848.
Solari, L.A., Garcia-Casco, A., Martens, U., Lee, J.K.W., Ortega-Rivera, A., 2013. Late Cretaceous subduction of the continental basement of the Maya block (Rabinal Granite, Central Guatemala): tectonic implications for the geodynamic evolution of Central America. Geological Society of America Bulletin 125, 625–639.
Spear, F.S., 1993. Metamorphic Phase Equilibria and Pressure–Temperature–Time Paths. Mineralogical Society of America Monographs, Washington.
Stanek, K.P., Maresch, W.V., Grafe, F., Grevel, C., Baumann, A., 2006. Structure, tectonics and metamorphic development of the Sancti Spiritus Dome (eastern Escambray massif, Central Cuba). Geologica Acta 4, 151–170.
Stern, R.J., 2010. The anatomy and ontogeny of modern intra-oceanic arc systems. In: Kusky, T.M., Zhai, M.G., Xiao, W. (Eds.), The Evolving Continents: Understanding Processes of Continental Growth. Geological Society of London, Special Publication Vol. 338, pp. 7–34.
Torres-Roldán, R.L., Garcia-Casco, A., García-Sánchez, P.A., 2000. CSpace: an integrated workplace for the graphical and algebraic analysis of phase assemblages on 32-bit Wintel platforms. Computers and Geosciences 26, 779–793.
Torró, L., Camprubí, A., Proenza, J.A., León, P., Stein, H.J., Nelson, C.E., Chavez, C., Villafaña, R., Lewis, J.F., Melgarejo, J.C., 2016a. Re-Os and U-Pb geochronology of the Doña Amanda and Cerro Kiosko deposits, Bayaguana district, Dominican Republic: looking down for the porphyry Cu-Mo roots of Pueblo Viejo-type mineralization in PIA series of the Caribbean. Economic Geology (accepted).
Torró, L., Proenza, J.A., Farré de Pablo, J., Colomer, J.M., Garcia-Casco, A., Melgarejo, J.C., Alfonso, P., Gubern, A., Gallardo, E., Cazañas, X., Chávez, C., del Carpio, R., León, P., Espaillat, J., Lewis, J.F., 2016b. Mineralogy, geochemistry and sulfur isotope characterization of Cerro de Maimón (Dominican Republic), San Fernando and Antonio (Cuba) Lower Cretaceous VMS deposits: formation during subduction initiation of the Proto-Caribbean lithosphere within a fore-arc. Ore Geology Reviews 72, 794–817.
Torró, L., Proenza, J.A., Garcia-Casco, A., Farré de Pablo, J., del Carpio, R., León, P., Chávez, C., Domínguez, H., Brower, S., Espaillat, J., Nelson, C.E., Lewis, J.F., 2016c. La geoquímica de la Formación Maimón (Cordillera Central, República Dominicana) revisada. Boletín Geológico y Minero (in press).
Vila, J.M., Boisson, D., Butterlin, J., Feinburg, H., Pubellier, M., 1987. Le complexe chaotique fini-éocène de Chouchou (Massif du Nord d'Haïti); un enregistrement du début des décrochements senestres nord-Caraibes. Comptes Rendus de la Académie des Sciences 304, 39–42.
Wakabayashi, J., Dilek, Y., 2000. Spatial and temporal relationships between ophiolites and their metamorphic soles: a test of models of forearc ophiolite genesis. In: Dilek, Y., Moores, E.M., Elthon, D., Nicolas, A. (Eds.), Ophiolites and Oceanic Crust: New Insights from Field Studies and the Ocean Drilling Program. Geological Society of America Special Papers Vol. 349, pp. 53–64.
West Jr., D.P., Abbott Jr., R.N., Bandy, B.R., Kunk, M.J., 2014. Protolith provenance and thermotectonic history of metamorphic rocks in eastern Jamaica: evolution of a transform plate boundary. Geological Society of America Bulletin 126, 600–614.
Whitney, D.L., Evans, B.W., 2010. Abbreviations for names of rock-forming minerals. American Mineralogist 95, 185–187.
Wiewióra, A., Weiss, Z., 1990. Crystallochemical classifications of phyllosilicates based on the unified system of projection of chemical composition: II. The chlorite group. Clay Minerals 25, 83–92.
Willner, A.P., Maresch, W.V., Massonne, H.J., Sandritter, K., Willner, G., 2016. Metamorphic evolution of blueschists, greenschists, and metagreywakes in the Cretaceous Mt. Hibernia Complex (SE Jamaica). European Journal of Mineralogy. http://dx.doi.org/10.1127/ejm/2016/0028-2561 (in press).